Mesoscale Influences of Wind Farms throughout a Diurnal Cycle

ANNA C. FITCH

Geophysical Institute, University of Bergen, and Uni Research, Bergen, Norway, and Mesoscale and Microscale Meteorology Division, National Center for Atmospheric Research, Boulder, Colorado

JULIE K. LUNDQUIST

Department of Atmospheric and Oceanic Sciences, University of Colorado, Boulder, and National Renewable Energy Laboratory, Golden, Colorado

JOSEPH B. OLSON

NOAA/Earth System Research Laboratory, and Cooperative Institute for Research in Environmental Sciences, Boulder, Colorado

(Manuscript received 1 July 2012, in final form 4 January 2013)

ABSTRACT

Large wind farms are expected to influence local and regional atmospheric circulations. Using a mesoscale parameterization of the effects of wind farms that includes a momentum sink and a wind speed–dependent source of turbulent kinetic energy, simulations were carried out to quantify the impact of a wind farm on an atmospheric boundary layer throughout a diurnal cycle. The presence of a wind farm covering 10 km × 10 km is found to have a significant impact on the local atmospheric flow and on regions up to 60 km downwind at night. Daytime convective conditions show little impact of the wind farm on wind speeds, as the momentum deficits generated by the wind farm rapidly mix through the depth of the boundary layer. At night, the stable layer within the rotor area inhibits turbulent mixing of the momentum deficit, leading to a shallower wake and a greater reduction in the wind speed within the wake. Although a low-level jet forms at altitudes within the rotor area in the hours before dawn, it is completely eliminated within the wind farm. At night, a maximum warming of 1 K is seen at the bottom of the rotor area. Near the surface, there is less warming (0.5 K). Downwind, the surface temperature perturbation is small, with a cooling of up to 0.3 K. Over the simulation period, the mean temperature change over the wind farm area at 2 m is a very slight warming (0.2 K). Mean temperature changes downwind are negligible. Other influences on turbulent kinetic energy, surface heat fluxes, and boundary layer height, are discussed.

1. Introduction

To harvest energy from the atmosphere, wind farms extract kinetic energy from the flow, inducing a perturbation in the ambient flow that may have the potential to impact the local weather and climate. The magnitude and spatial extent of this impact are largely unknown because few direct observations exist, and the perturbations are expected to vary widely as a function of atmospheric conditions, local vegetation, terrain, and turbine types. Furthermore, the perturbation induced by wind farms on the atmosphere can feed back on the wind farm operations, affecting the efficiency of power production. A detailed understanding of this atmosphere–wind farm interaction is an important research need that will aid in wind farm operations, and may also influence public acceptance of large wind farms, and therefore, the future growth of the wind energy market.

Unfortunately, there are few observational reports available to quantify the three-dimensional impacts of wind farms on local wind, turbulence, temperature, or moisture; the few that are available are primarily focused on remote sensing of surface characteristics. Christiansen and Hasager (2005) employed synthetic aperture radar (SAR) to investigate the wake from the Horns Rev and Nysted wind farms in Denmark. An 8%–9% reduction in the wind at a height of 10 m was observed immediately downwind of the wind farms. The recovery of the wake

Corresponding author address: Anna C. Fitch, National Center for Atmospheric Research, P.O. Box 3000, Boulder, CO 80307.
E-mail: fitch@ucar.edu

DOI: 10.1175/MWR-D-12-00185.1

was dependent on atmospheric stability, with a faster recovery in unstable conditions under which the wake persisted only 5 km downwind. In neutral conditions, however, the wake extended more than 21 km downwind. Turbulence intensity was increased at the surface downwind in approximately one-third of the cases studied. Jensen (2007) considered the power output from the Horns Rev wind farm, finding wake impacts on turbine efficiency were larger during stable conditions. Similarly, Barthelmie and Jensen (2010) considered the power output from the Nysted wind farm, and found stable conditions led to reduced efficiency in the power output of the farm. The lower ambient turbulence in stable conditions led to slower mixing of the momentum deficit within the wake. Hansen et al. (2012) confirmed previous analyses of Horns Rev, again demonstrating that the power deficit was a function of ambient turbulence intensity. As turbulence intensity increased, the power deficit decreased. The more stable the conditions were, the larger the power deficit. The wake was wider and deeper during very stable conditions, caused by decreased turbulent mixing of the wake. Observations at the research farm at the ECN Wind Turbine Test Site Wieringermeer (EWTW) also indicate greater wake deficits during conditions with low turbulence (Schepers et al. 2012), as have previous observations of wakes of individual turbines (Högström et al. 1988, among others).

Wind farms have been found to influence temperature in addition to wind and turbulence. In considering observations from the San Gorgonio wind farm, Baidya Roy and Traiteur (2010) found near-surface air temperatures within and downwind of the farm were modified. During stable stratification of the low-level air, the wind farm induced a slight warming; conversely, an unstable stratification led to cooling. Zhou et al. (2012) analyzed radiometric surface temperatures derived from satellite radiometric observations within and downwind of wind farms in west Texas. When considering clear-sky conditions over 9 years, they observed a warming of less than 1°C during nighttime conditions. A small warming was seen during the daytime. However, although they analyzed the potential influence from the local terrain, they were not able to completely rule out the influence of terrain variations on their results.

To help fill the observational gaps, further inquiries into the impacts of wind farms have been performed with numerical modeling experiments. A variety of modeling techniques have been used to represent the interactions of wind turbines with atmospheric flow. In decreasing order of sophistication, these approaches are categorized as 1) representing individual turbines using computational fluid dynamics or large-eddy simulations (LES), 2) representing individual turbines or aggregates of turbines using mesoscale models, and 3) representing wind farms as a whole in global models, typically using a highly simplified enhancement of the surface roughness lengths.

In the first category, Calaf et al. (2010) quantify the vertical transport of momentum and kinetic energy (KE) associated with wind turbines modeled using an actuator (drag) disk approach with LES in a neutral boundary layer (BL). The vertical fluxes of KE were found to be of the same order of magnitude as the power extracted by the turbines. Cal et al. (2011) confirmed these results by performing a wind-tunnel experiment with model wind turbines. In addition, Calaf et al. (2010) found a peak in turbulence production at the top of the turbines. In their LES using an actuator line technique to model a wind turbine in a stable BL, Lu and Porté-Agel (2011) found enhanced vertical mixing caused by the turbine led to an increase in temperature within the rotor area of approximately 0.5 K. Above the turbine, the temperature decreased by up to 1 K, while little temperature change was found at the surface. Surface heat fluxes were reduced by more than 15% and the surface momentum flux was reduced by more than 30%. In addition, the low-level jet (LLJ) within the rotor area was eliminated because of energy extraction, and the height of the shallow BL increased from enhanced mixing by the turbine. Calaf et al. (2011) extended their previous LES study to explore the influence of wind turbines on scalar transport in a neutral BL, and found an increase of 10%–15% in the scalar fluxes at the surface when wind turbines were present. Momentum transport was enhanced above the farm (increased friction velocity) and dominated a slightly reduced momentum transport near the surface (reduced friction velocity), leading to a small increase in the scalar flux near the surface in these neutrally stratified simulations. The impact of stratification on these results was not explored.

The impact of atmospheric stability and surface roughness on wake recovery and power production was studied by Churchfield et al. (2012) using an actuator line technique to represent two wind turbines in LES. The ratio of the power produced by the downwind turbine relative to the upwind turbine was 15%–20% higher in unstable conditions compared to neutral conditions, as a result of the enhanced mixing in convective conditions. For a given stability, the power ratio was 10% higher, with greater surface roughness representing land, than with lower surface roughness representing water. The increased surface roughness enhanced turbulent mixing, leading to a faster wake recovery. The large computational resources needed for LES limited the number of turbines in the study, as well as the ability to assess the impacts far downwind.

Impacts similar to those observed with LES have been found using techniques in the second category. In this approach, a wind farm is represented as an elevated momentum sink and source of turbulence (turbulent kinetic energy) using mesoscale or limited-area models. Studies using this technique were performed by Baidya Roy et al. (2004), Adams and Keith (2007), Baidya Roy and Traiteur (2010), Blahak et al. (2010), Baidya Roy (2011), Fiedler and Bukovsky (2011), and Fitch et al. (2012). These modeling approaches differ according to how the momentum sink and turbulent kinetic energy (TKE) produced by the wind farm are quantified. For an overview of these approaches, see Fitch et al. (2012). Baidya Roy et al. (2004) found wind turbines enhanced vertical mixing of momentum and heat. Warming of the surface occurred during stable stratification, and cooling of the surface occurred with unstable stratification. The impact on near-surface air temperature was greater when the source of TKE from the turbines was increased. However, the downwind impacts appeared to persist only 18–23 km from the downwind edge of the farm for the two stable cases explored (Baidya Roy 2011). Fiedler and Bukovsky (2011) found the presence of a theoretical giant wind farm covering 182 700 km^2 in the central United States caused a great impact on the warm-season precipitation in the eastern two-thirds of the United States, for one season. This impact is consistent with the known sensitivity of weather to initial conditions. However, when the mean impact over 62 years of simulations was considered, only a 1% enhancement of precipitation was found surrounding and to the southeast (downwind) of the farm. A possible explanation given was the wind farm could somewhat retard advection of drier air from the northwest. Fitch et al. (2012) modeled an idealized offshore wind farm covering 10 km $\times$ 10 km, and found a wind speed deficit extending throughout the depth of the neutral BL, above and downwind from the farm, with a long wake of 60 km *e*-folding distance. However, the near-surface winds within the wind farm (under the turbine rotor disks) were accelerated by up to 11%. A maximum increase of TKE, by nearly a factor of 7, was located within the farm, and a significant enhancement in the turbulent momentum fluxes was seen. No studies with mesoscale models have yet been performed to show how these impacts vary within a diurnal cycle, but this variability will be addressed herein.

For global simulations in the third category, wind farms are represented with areas of increased surface roughness, as Ivanova and Nadyozhina (2000), Keith et al. (2004), Kirk-Davidoff and Keith (2008), Barrie and Kirk-Davidoff (2010), and Wang and Prinn (2010, 2011) discussed. In a global climate model, Keith et al. (2004) found theoretical wind farms covering large areas caused a negligible change in the global mean surface air temperature. However, local maxima of temperature changes exceeding ± 2°C did occur. Kirk-Davidoff and Keith (2008) found surface roughness anomalies covering large areas representing wind farms generated appreciable wind, temperature, and cloudiness anomalies. Barrie and Kirk-Davidoff (2010) showed the initial disturbance generated by a large wind farm induced a synoptic response. With a global coupled atmosphere–ocean climate model, Wang and Prinn (2010) found temperatures warmed by 1°C over onshore wind farms, and cooled by 1°C over offshore wind farms, with the warming limited to the lowermost layers in the atmosphere. Ocean–atmosphere heat fluxes increased in response to increased turbulence in the wind farm areas. These results generally imply larger impacts than those from other methods, warranting further research to validate this method.

While LES can provide insight into the complex interaction between individual turbines and the boundary layer, until now it has been too computationally expensive to simulate wind farms with large numbers of turbines and the resulting wakes far downwind. Mesoscale numerical weather prediction (NWP) models provide an opportunity to investigate the flow in and around large wind farms as a whole, and thereby assess the resulting impact on local and regional meteorological conditions. For this purpose, we implemented a wind farm parameterization (Fitch et al. 2012) in the Weather Research and Forecasting Model (WRF) (Skamarock et al. 2008), which represents wind turbines by imposing a momentum sink on the mean flow, converting kinetic energy into electricity and TKE. This parameterization method falls within the second category, but improves upon previous models by basing the atmospheric drag of turbines on the thrust coefficient of a modern commercial turbine. In addition, the source of TKE varies with wind speed, reflecting the amount of energy extracted from the atmosphere by the turbines that does not produce electrical energy. The parameterization is discussed in detail in Fitch et al. (2012).

Local impacts of wind farms are expected to vary with atmospheric stability, because wake impacts on downwind turbines have been shown to vary with stability. To explore how a wind farm may affect its local environment in a range of stability conditions, we posit a hypothetical wind farm in Kansas, in the midwestern United States, a region of considerable wind farm deployment. We force the diurnal cycle with observations from the 1999 Cooperative Atmosphere–Surface Exchange Study (CASES-99) program (Poulos et al. 2002) for a well-studied and oft-simulated 2-day period discussed in detail in Svensson et al. (2011). We consider a wind farm covering

10 km × 10 km over land containing 100 turbines. The model configuration is further described in section 2. The impacts of the wind farm on wind velocity, turbulent mixing, temperature, and surface heat flux are discussed in section 3. Section 4 discusses the primary results and compares them with those available from observations and from large-eddy simulations. The results from this investigation are the first to detail the important three-dimensional structures caused by the atmosphere–wind farm interaction, and how these structures evolve throughout the diurnal cycle.

2. Experimental method

a. Model configuration

The aim of the present work is to explore the interaction between a large wind farm and the boundary layer throughout a diurnal cycle. To this end, a well-studied case is chosen in an area characteristic of where wind farm development is planned. The second model intercomparison case study within the Global Energy and Water Cycle Experiment Atmospheric Boundary Layer Study (GABLS2; Svensson et al. 2011) simulates a strong diurnal cycle in a region of the U.S. Midwest in Kansas. This case is based on observations collected during the CASES-99 (Poulos et al. 2002) in October 1999. The methodology in Svensson et al. (2011) is used to provide the initial conditions and forcing to simulate the diurnal cycle using the mesoscale numerical weather prediction model, the Advanced Research WRF (ARW; version 3.3.1; Skamarock et al. 2008).

The simulation begins at 1400 local time (LT) 22 October 1999 and runs for 59 h. The model is initialized with a uniformly flat surface with an aerodynamic roughness length of 0.03 m, characteristic of the prairie grassland in the area. An *f* plane is used, with the Coriolis parameter set according to the case location of 37.6°N, 96.7°E. The surface pressure is 972 hPa. The model is initialized with horizontally uniform profiles of potential temperature, specific humidity, and TKE. The evolution of the BL is forced by a prescribed surface skin temperature, defined by a sinusoidal function during the daytime and a linear function at night, as in Svensson et al. (2011). The geostrophic wind forcing is constant over time, with the zonal and meridional components of the geostrophic wind set to 3 and -9 m s^{-1}, respectively, at all levels. A small amount of subsidence, dependent on height, is introduced after 1600 LT 23 October, and is of maximum 0.005 m s^{-1}. For additional details, see Svensson et al. (2011).

The domain configuration and physical parameterizations used in the simulation are the same as in Fitch et al. (2012), and the reader is referred to that paper for full details. A two-way nested grid configuration is employed in order to ensure minimal interaction with the lateral boundaries. The coarse and fine grids both have dimensions of 202 × 202 points, with 3- and 1-km horizontal resolution for the coarse and fine grids, respectively. The fine grid is centered inside the coarse grid. In the vertical, the levels are progressively stretched toward the top, with 81 levels in total, and 30 levels below 1 km. There are eight levels intersecting the rotor area [see Fig. 1 in Fitch et al. (2012)]. The model top is at 20 km, and a Rayleigh relaxation layer of 5-km depth controls gravity wave reflection. Open radiative lateral boundary conditions are used on all boundaries of the coarse grid, following the method of Klemp and Wilhelmson (1978). For the fine grid, the boundary conditions are interpolated from the coarse grid at the outermost rows and columns of the fine grid. The time step is 9 and 3 s for the coarse and fine grids, respectively.

The physical parameterizations are configured to isolate the turbulent mixing induced by the wind farm, with only the planetary boundary layer (PBL) physics and surface layer fluxes active. There are no clouds present in the case; therefore, the microphysics scheme is turned off. Because the diurnal evolution of the BL is forced by the prescribed surface skin temperature, the radiation scheme is also turned off. The PBL physics are parameterized using the Mellor–Yamada–Nakanishi–Niino (MYNN) model (Nakanishi and Niino 2009). The scheme was chosen in part because LES was used to determine the fundamental closure constants, and the prediction of TKE was tuned to match LES, resulting in a more reliable prediction of TKE. This property is important for coupling to the wind farm parameterization.

A new diagnostic for determining the PBL height is employed in these simulations to improve estimates over the full diurnal range. This method is best described as a hybrid-PBL height diagnostic, which uses the virtual potential temperature θ_v-based definition of Nielsen-Gammon et al. (2008) for unstable conditions, and a TKE-based threshold definition under stable conditions. The θ_v-based approach estimates the PBL height to be the height at which $\theta_v = \theta_{v,\min} + 1.5$, where $\theta_{v,\min}$ is the minimum θ_v in the lowest 500 m. This method has been shown to produce PBL height estimates that are unbiased relative to profiler-based estimates of daytime convective PBL heights (Nielsen-Gammon et al. 2008). Nocturnal conditions, without strong surface-based forcing, require a different approach. Banta et al. (2003) show that a TKE-based threshold diagnostic can be a good estimate of the PBL height during LLJ events, such as those occurring in this study. The TKE-based diagnostic used here estimates the PBL height to be the height at which

the TKE becomes less than $\varepsilon_{\mathrm{TKE}}$, where $\varepsilon_{\mathrm{TKE}} = \mathrm{TKE}_{\mathrm{max}}/20$ and $\mathrm{TKE}_{\mathrm{max}}$ is the maximum TKE in the lowest 500 m. The variable TKE threshold, $\varepsilon_{\mathrm{TKE}}$, is used, as no particular value was found to work best for all conditions. The hybrid PBL height definition incorporates both methods, determining the weight for each method solely from the θ_v-based PBL height, which is a good proxy for the low-level static stability. The hybrid PBL height, $z_{i,\mathrm{hybrid}}$, is given by

$$z_{i,\mathrm{hybrid}} = W z_{i,\theta_v} + (1 - W) z_{i,\mathrm{TKE}}, \tag{1}$$

and

$$W = 0.5 \tanh\left(\frac{z_{i,\theta_v} - z_{i,\mathrm{stable}}}{2 z_{i,\mathrm{stable}}}\right) + 0.5, \tag{2}$$

where z_{i,θ_v} is the PBL height given by the θ_v-based definition, $z_{i,\mathrm{TKE}}$ is the PBL height given by the TKE method, and $z_{i,\mathrm{stable}}$ (=200 m) is a typical height of a strong nocturnal inversion. Therefore, the TKE-based method is weighted more in stable conditions (when the θ_v-based diagnostic becomes less than 200 m), while the θ_v-based approach has a larger weight in convective conditions. In neutral conditions, the θ_v-based approach typically dominates.

b. Wind farm configuration

The wind farm is parameterized following the approach used by Fitch et al. (2012). The parameterization represents the influence of wind turbines on the atmosphere by imposing a momentum sink on the mean flow, at model levels within the rotor area. A fraction of the KE extracted from the mean flow produces electricity, and the rest is transformed into TKE. The wind turbine thrust coefficient quantifies the total fraction of KE extracted by the turbines, and is a function of the wind speed and turbine type. The fraction of this energy, which ultimately generates electricity, is given by the power coefficient. Both of these proprietary coefficients are measured by the turbine manufacturer, and were formulated in the model by fitting a function to the curves to define the coefficients for a given wind speed.

A large wind farm of size 10 km × 10 km is placed at the center of the fine grid, consisting of 100 turbines, each with a nominal power output of 5 MW. A typical turbine spacing of eight rotor diameters is used, with one turbine per grid cell. The turbines modeled are based on the thrust and power coefficients of the REpower 5M turbine. These turbines have a hub height of 100 m, and a blade diameter of 126 m. The cut-in and cut-out wind speeds, below and above which the turbines do not operate, are 3.5 and 30 m s^{-1}, respectively. Between the cut-in speed and 9 m s^{-1}, the thrust coefficient is a maximum and mostly constant with wind speed. At higher wind speeds, the thrust coefficient falls rapidly, and at 13 m s^{-1} (the maximum wind speed in the simulation), the thrust coefficient is approximately half the value at lower speeds.

3. Results

a. Evolution of the case

To study the interaction of a large wind farm with the boundary layer over a diurnal cycle, we performed two experiments with the GABLS2 case: one in which no wind farm was present (denoted NF), and a second with a wind farm covering 10 km × 10 km using the configuration described in section 2b (denoted CTRL). The impact of the wind farm is highlighted by taking the difference between the two experiments. The first 12 h of the simulations are discarded to eliminate spinup effects in the model. Profiles are averaged over the wind farm area, and over an area equal in size to the wind farm (10 km × 10 km) 10–20 km downwind of the wind farm. The downwind region is defined by the mean wind direction at hub height in the NF case. To elucidate the physical mechanisms involved in the perturbation induced by the wind farm, an additional two experiments were carried out with part of the parameterization turned off. In one experiment, the elevated momentum sink was kept active, but without any source of TKE. In another experiment, the momentum sink was turned off, with only the source of TKE active.

The overall evolution of the BL over two days, without the wind farm present, is shown in Fig. 1a. The prescribed skin temperature cools gradually throughout the night, building a stable layer adjacent to the ground that reaches a maximum at dawn, at 0600 LT the first day. At this time, the BL is stably stratified to the top of the rotor area, and the height of the BL reaches a minimum of 58 m (red line), as defined by the hybrid PBL height [Eq. (1)]. The wind speed is weakest within the rotor area during the morning transition (0600–0900 LT), with a minimum of 4.6 m s^{-1} at hub height at 0900 LT on the first day. As the ground surface warms after dawn, the stable layer is gradually eroded until 1000 LT, when it has been eliminated completely. The BL is unstable after this time during the day, and reaches a maximum of 964 m at 1500 LT. Large-scale subsidence introduced after 1600 LT causes the upper region of the BL to gradually warm (indicated by the downward-sloping isentropes at upper levels of the BL in Fig. 1a). From 1600 LT, the ground surface begins to cool and a stable layer reforms

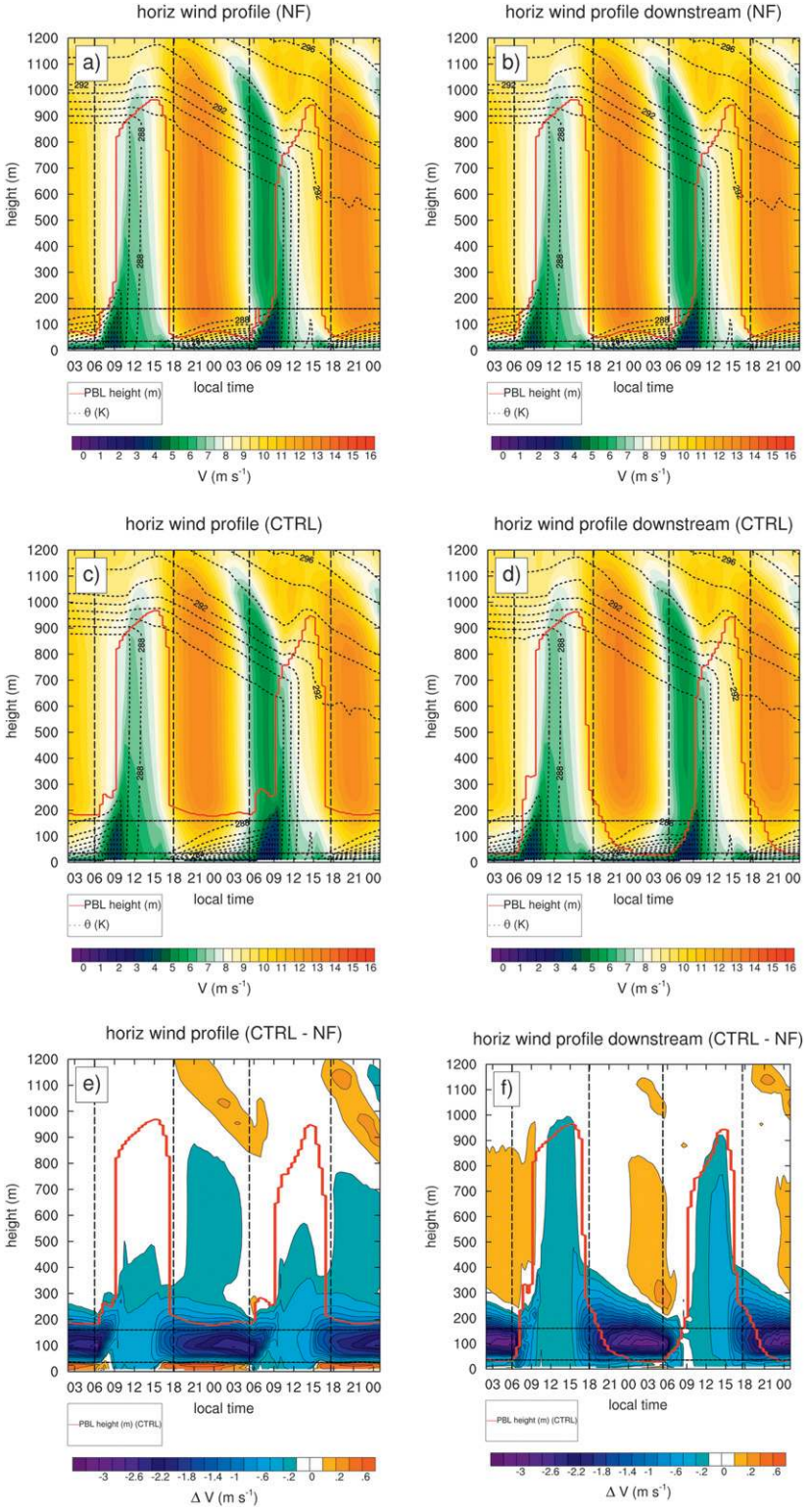

FIG. 1. Evolution of mean wind and potential temperature profiles and PBL height over the wind farm area: (a) without the wind farm, (c) with the wind farm, (e) the difference in wind speed. Evolution of mean wind and potential temperature profiles and PBL height 10–20 km downwind of the wind farm: (b) without the wind farm, (d) with the wind farm, and (f) the difference in wind speed. Vertical dashed lines indicate sunrise and sunset times; horizontal lines indicate the extent of the rotor area.

throughout the night, growing from a minimum depth of 54 m to a maximum of 125 m just before dawn at 0530 LT. The wind becomes supergeostrophic after 1700 LT on the first day between the hub height and the top of the residual BL [approximately 1000 m above ground level (AGL)]. This deep layer of accelerated flow eventually reaches a maximum wind speed at hub height of 13.2 m s^{-1}, at 2230 LT. As the stable layer develops, the supergeostrophic wind in the residual layer becomes decoupled from the surface, forming a LLJ near the top of the rotor area after 0000 LT (more clearly visible in Fig. 4a). Note that the overall wind speed decelerates over the night, which also occurred in other GABLS simulations (W. Angevine 2012, personal communication). The LLJ begins to decay as the prescribed skin temperatures start to warm and the BL height builds on the second day.

The wind speed at hub height is always above the cut-in speed of the turbines, at which the turbines are operating, but only marginally during the morning transition on the second day. The variation of the wind speed on the second day follows a similar pattern as the first, with the wind speed reaching a maximum of 12.9 m s^{-1} at hub height at 2130 LT. An LLJ is again present within the vicinity of the turbine blades after 0000 LT. During both nights, the height of the BL is determined primarily by the TKE-based component of the hybrid PBL height diagnostic, and is below the height of the top of the turbines (163 m). During the second day, the stable layer is completely eroded by 1000 LT and is again unstable afterward, until surface cooling begins at 1500 LT and a stable layer once again grows. The subsidence causes the maximum BL height to be lower on the second day, at 945 m (1430 LT).

The evolution of the BL over two days, in the presence of the wind farm, is shown in Fig. 1c. To highlight the impact of the wind farm, the difference between the CTRL and NF cases is shown in Fig. 1e. The wind turbines remove momentum, leading to a reduction of the wind within the rotor area. The greatest reduction in the wind is seen during the night when wind speeds are higher, the turbines produce more power, and turbulent mixing is inhibited by the stable stratification. This reduction grows until dawn, up to a maximum of 2.4 m s^{-1} at hub height at 0600 LT on the first day, representing a reduction of 22%, relative to the NF simulation. The wind reduction is smallest during the middle of the day when the turbines produce less power, and turbulent mixing is greatest, with a reduction of only 0.2 m s^{-1} (3.5%) at hub height at 1100 LT on the first day. From late afternoon until dawn, an acceleration of the wind is seen below the rotor area. This acceleration is of maximum 0.8 m s^{-1}, an increase of 10% relative to NF. The acceleration is greatest just below the rotor area at a height of around 30 m. Closer to the ground, at 10 m AGL, the wind is increased by less than 0.4 m s^{-1}, an increase of 10%–15% relative to NF. The acceleration below the rotor area is due to the source of TKE within the wind farm, which increases turbulent mixing, transporting air with higher momentum downward. The acceleration in the near-surface wind is not present when only the momentum sink component of the wind farm parameterization is active, owing to an unfavorable pressure gradient. When the source of TKE is active, the pressure gradient becomes more favorable, also acting to accelerate the wind, in addition to vertical mixing.

In the hours before dawn, the LLJ, which occurs at the height of the rotor area in the NF case, is eliminated in the CTRL case because of the extraction of momentum by the turbines; this behavior is discussed in more detail in section 3c. This wind speed reduction extends up to a height of 700–900 m at night and 400–600 m during the day. The BL height is increased significantly above the wind farm during the night, similar to that in the study by Lu and Porté-Agel (2011), by up to 145 m, an increase by a factor of over 4 relative to NF, at 0500 LT on the second day. In contrast, the BL height remains relatively unchanged during the day. The depth of the stable layer is increased by the production of TKE by the wind farm at night, along with a small reduction in the strength of the stratification, owing to the increased turbulent mixing induced by the wind farm. This change in low-level stratification by the enhanced turbulent mixing is discussed in more detail in section 3f.

The evolution of the BL 10–20 km downwind of the wind farm is shown in Fig. 1b (NF) and Fig. 1d (CTRL), with the difference between the CTRL and NF cases shown in Fig. 1f. Note the NF simulation is horizontally uniform, thus the profile over the farm (Fig. 1a) is the same as the profile downwind (Fig. 1b). At a distance of 10–20 km downwind from the wind farm, the wind speed has not yet recovered from the momentum deficit created by the extraction of momentum from the wind farm. The greatest reduction of the wind at hub height is seen in the hours before dawn, with a maximum reduction of 3.0 m s^{-1} (28% relative to NF) at 0600 LT on the first day. The downwind reduction averaged over an area 10–20 km downwind is larger than that averaged over the area of the farm, as downwind, all the turbines have extracted energy. During the daytime, the wind deficit is mixed throughout the depth of the BL, but is much smaller in magnitude, with a maximum deficit of 0.2 m s^{-1}, than at night. As the wind speed within the rotor area increases in the afternoon hours, the turbines extract more momentum, leading to a greater deficit in the wind. The wake is initially deep, with a depth of around 400 m at 1600 LT. Throughout the evening and night, the wake becomes shallower (shown by the downward sloping

isotachs during the night in Fig. 1f) as the stable layer grows in depth and inhibits vertical mixing. A region of accelerated flow develops at a height of between 200 and 900 m after 0000 LT, and is associated with subsidence forced by decelerated flow within the farm, which transports high momentum air from upper levels down, at the rear of the farm.

TKE affects the evolution of the flow around the wind farm, and is produced directly by the wind farm parameterization, as well as through shear and buoyancy production via the PBL scheme. The evolution of TKE within the BL is shown for the NF case in Fig. 2a. The greatest TKE is seen during the day, where buoyancy production in the unstable BL allows turbulent mixing to spread throughout the depth of the BL. A maximum in TKE of 1.5 $m^2 s^{-2}$ occurs around 1200 LT. As the ground surface cools from late afternoon throughout the night, the stable stratification inhibits turbulence and a minimum in TKE of 0.1 $m^2 s^{-2}$ is seen close to the ground. The evolution of TKE in the presence of the wind farm is shown in Fig. 2b, with the difference between the CTRL and NF cases shown in Fig. 2c. During the daytime, the wind farm causes an increase in TKE, which is efficiently mixed throughout the depth of the BL, with a maximum of 2.0 $m^2 s^{-2}$ (an increase of 0.5 $m^2 s^{-2}$, or 33% relative to NF) in the upper half of the rotor area around 1200 LT on the second day. At night when ambient turbulence is low, and most power is produced, there is a significant increase of TKE relative to NF within the rotor area, and also above to a height of around 250 m. A maximum in TKE of 1.0 $m^2 s^{-2}$, an increase by a factor of 20 relative to NF, is seen in the upper half of the rotor area from around 1800 to 0000 LT. This increase is caused not only by the direct addition of TKE by the wind farm parameterization, but also indirectly, by the wind shear induced by the momentum sink. The smallest amount of TKE within the rotor area is observed during the morning transition of the second day, when power production is minimal.

b. *Mean wake structure*

The mean perturbation induced by the wind farm during the day and night is shown in Fig. 3, both in the horizontal and vertical. During the day, the wind in the rotor area is weaker than at night, leading to lower power production and a smaller momentum deficit. The wake is weaker and persists for a shorter distance downwind than at night as a result (Figs. 3a,b). In addition, the unstable stratification during the day more quickly mixes the momentum deficit within the wake than at night with stable stratification. A maximum deficit of 0.8 m s^{-1}, a reduction of 10% relative to NF, occurs during the day at hub height toward the downwind edge of the farm. At

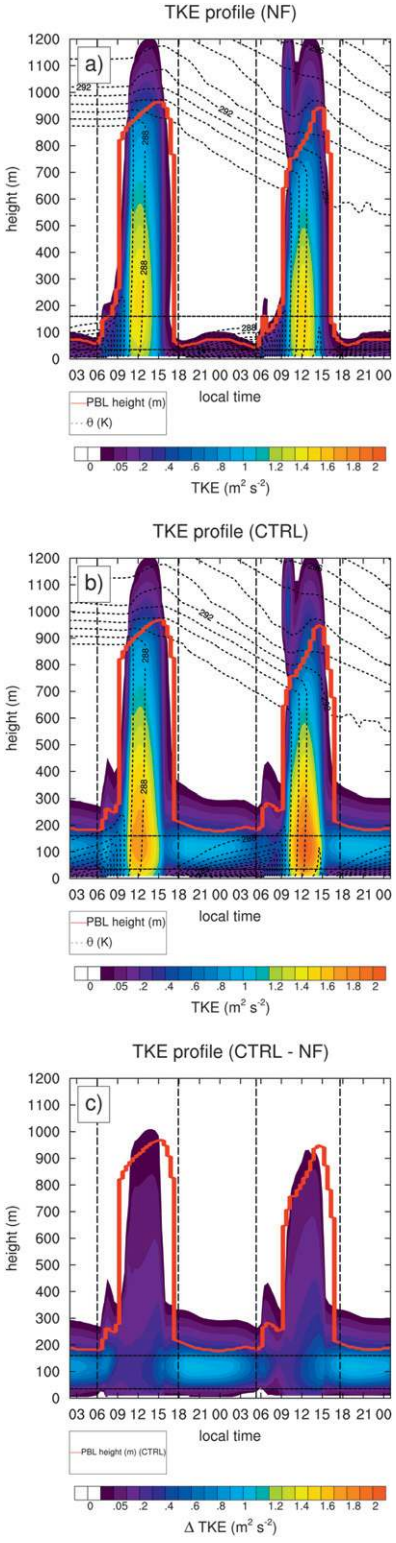

FIG. 2. Evolution of mean TKE and potential temperature profiles and PBL height over the wind farm area: (a) without the wind farm, (b) with the wind farm, and (c) the difference in TKE. Vertical dashed lines indicate sunrise and sunset times; horizontal lines indicate the extent of the rotor area.

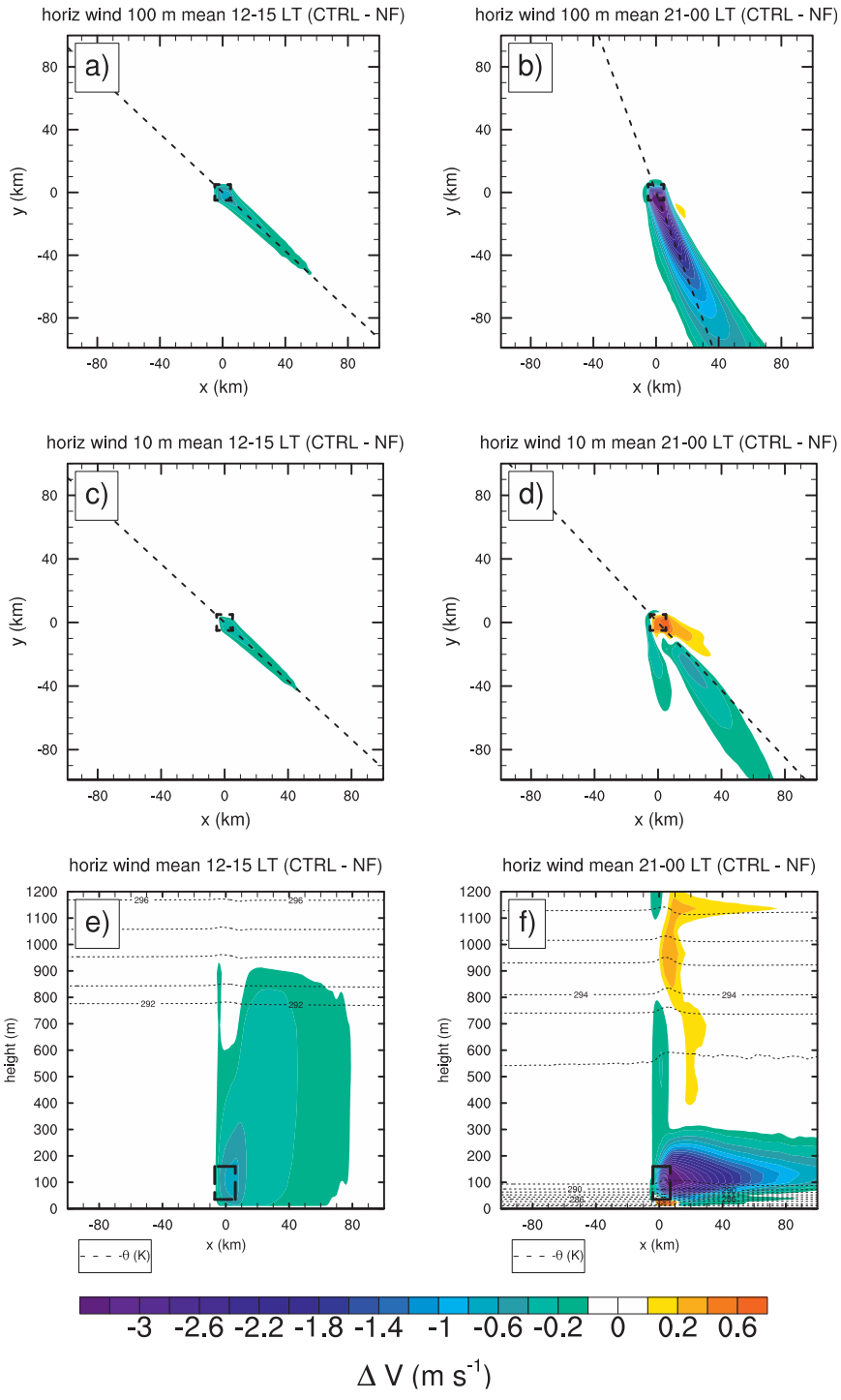

FIG. 3. Mean wake structure during the daytime, showing the horizontal wind speed difference between the wind farm (CTRL) and no-wind farm (NF) cases: (a) horizontal cross section at hub height (100 m), (c) horizontal cross section at 10 m, and (e) vertical cross section along the dashed line in (a). Mean wake structure during the nighttime: (b) horizontal cross section at hub height (100 m), (d) horizontal cross section at 10 m, and (f) vertical cross section along the dashed line in (b). Dashed rectangles indicate the wind farm area; straight dashed lines indicate the direction of the mean incoming northwesterly flow.

night, the maximum deficit increases to 3.8 m s^{-1}, a reduction of 30% at hub height. The wake has an *e*-folding distance of 15 km during the day at hub height, and increases by nearly a factor of 4, to 55 km at night. A 10% deficit in the wind persists for 60 km downwind at hub height during the night. There is a small deceleration (by 0.1 m s^{-1}) ahead of the farm, up to 2–3 km upwind during the night, owing to the convergence of the incoming flow and the inhibition of vertical motion in the stable layer.

The wake structure at 10 m above the ground is similar to that at hub height during the day, but is very different at night (Figs. 3c,d). There is a maximum reduction in the wind of 0.4 m s^{-1} (6%) during the day, and 0.5 m s^{-1} (11%) at night. This maximum is located at the downwind edge of the farm during the day, however, during the night, the wind is accelerated beneath the rotor area, and the maximum deficit is not seen until after 20 km downwind of the farm. The wind is accelerated by up to 0.9 m s^{-1}, an increase of 19%, toward the downwind edge of the farm. The flow on the left-hand side (lhs) of the wake (looking downwind) is accelerated, and decelerated on the right-hand side (rhs) owing to the divergence and convergence of the flow on the lhs and rhs, respectively. The divergence causes vertical transport of faster air aloft downward on the lhs. This effect is discussed in more detail in section 3d.

The vertical structure of the wake during the day is shown in Fig. 3e, and at night in Fig. 3f. During the day, the unstable stratification and associated turbulent mixing leads to the momentum deficit being spread throughout the depth of the BL, to a height of 800–900 m. A smaller reduction in the wind occurs as a result. At night, the stable layer within the rotor area inhibits turbulent mixing of the momentum deficit, leading to a shallower wake and a greater reduction in the wind. At the downwind edge of the farm, the wake is around 300 m deep. Convergence of air within the rotor area forces vertical motion above the wind farm, transporting slower air from lower levels upward. A column of decelerated flow results above the wind farm (Fig. 3f). The impinging vertical motion on the inversion at upper levels generates a gravity wave. At the downwind edge of the farm, subsidence transports faster-moving air at upper levels downward.

The wake behavior evolves slowly during the daytime and at night. However, during the transition periods, the wind farm wake behavior changes dramatically, as discussed in the following sections.

c. Interaction with the low-level jet

The nocturnal LLJ provides a tremendous wind resource to the midwestern United States. The simulations presented here show the wind farm impacts the LLJ within the farm area and downwind. Vertical profiles of the horizontal wind component averaged over the farm area between 2200 and 0600 LT on the first full night are shown in Fig. 4a. Without the wind farm, around 2200 LT, the supergeostrophic flow reaches its maximum speed in a deep layer from hub height to around 1000 m AGL; the shape of the profile does not yet indicate a jet. Over the night, the bulk layer wind speed decelerates, as observed with this case by Svensson et al. (2011). As the night progresses in the NF simulation, a subtle increase of wind speed at 150 m AGL, compared with winds above and below, forms. At 0000 LT, this increased wind speed is approximately 0.5 m s^{-1}. Although the wind profile as a whole decelerates overnight, this layer of relatively faster flow becomes more pronounced in comparison with the rest of the profile over time. By 0600 LT, this ''nose'' of the jet is 2 m s^{-1} faster than the layer above it in the NF case, qualifying as a LLJ by the criteria of Whiteman et al. (1997). In this case, the height of maximum LLJ wind speed is around 100 m AGL in the NF case, and most of the LLJ is confined to regions below 350 m.

When the wind farm is present, energy extraction by the turbines causes a considerable reduction in the wind, eliminating the LLJ within the rotor area. The layer below the turbine rotor disk is accelerated relative to the NF profile, with the strong velocity gradients somewhat weakened from the bottom of the rotor disk down to the surface. Differences between the CTRL case and the NF case persist up to approximately 300 m above the surface or approximately 150 m above the top of the rotor area, driven by mixing caused by the turbulence produced in the wake. Slight differences between the CTRL and NF cases persist up to 1200 m. The reduction in the wind in CTRL reaches a maximum of 2.0 m s^{-1} when the LLJ is most pronounced just before dawn (0600 LT). The stable layer is deepest at this time, inhibiting vertical mixing. Furthermore, the reduced wind shear above the rotor area owing to weaker flow aloft slows the exchange of momentum, inhibiting the recovery of the LLJ from the wind farm wake.

Downwind of the wind farm at a distance of 10–20 km (Fig. 4b), there is little recovery in the wind speed. The mean wind speed deficit over an area equal to the wind farm, 10–20 km downwind is increased slightly between 2200 and 0200 LT, relative to the profile over the wind farm itself. At this distance, all the turbines in the wind farm have extracted energy. Ekman turning advects the wake in the lower half of the rotor area at an angle away from that at hub height after 0400 LT. Therefore, a smaller wind deficit is seen at these levels, as the wind direction at hub height defines the region where the profile is taken.

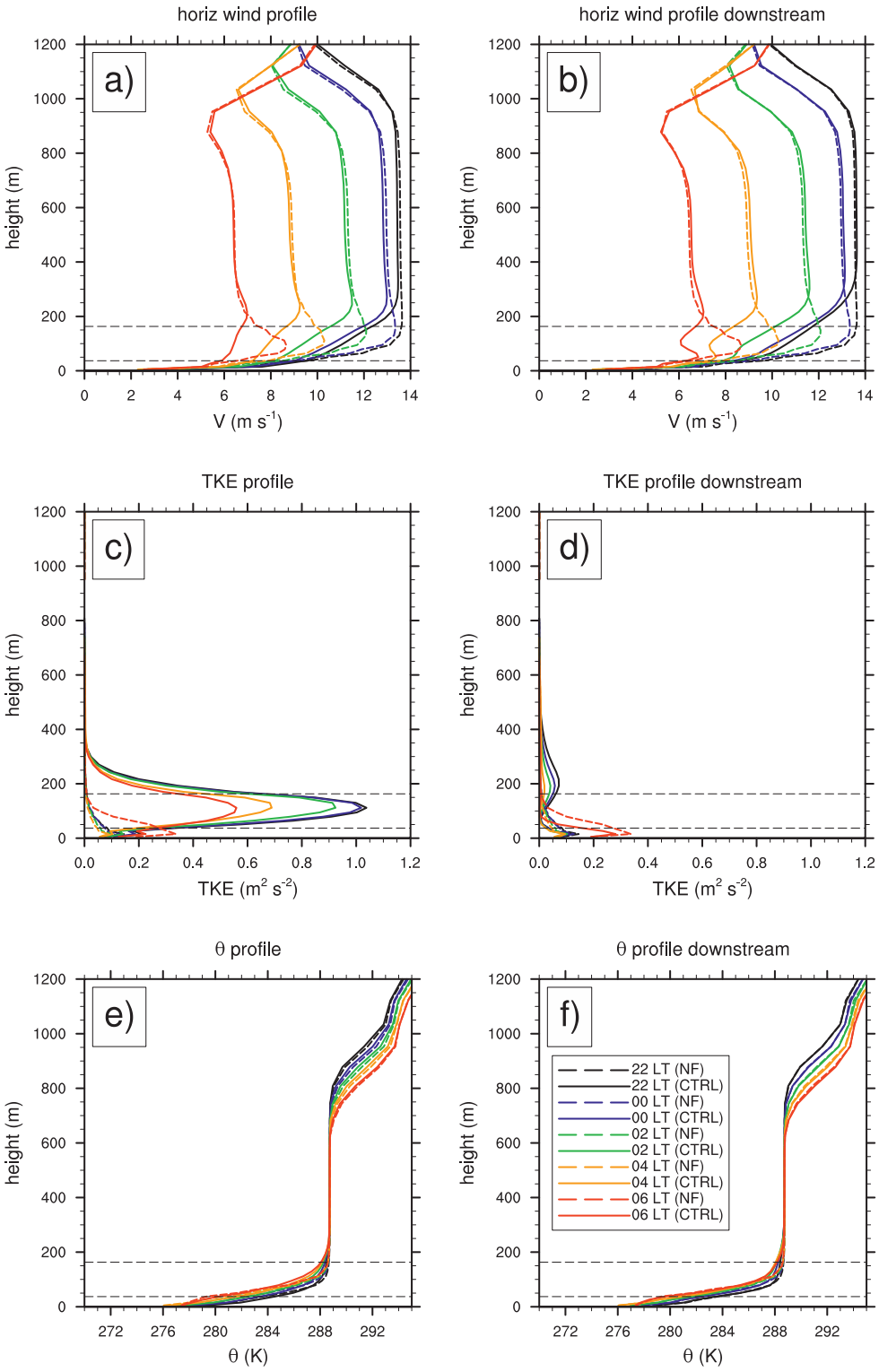

FIG. 4. Mean profiles over the wind farm area and downwind of the wind farm area during the LLJ on the night of 23–24 Oct showing the wind farm (CTRL) and no-wind farm (NF) cases: (a) horizontal wind speed profile over the wind farm area, (b) horizontal wind speed profile 10–20 km downwind of the wind farm area, (c) TKE profile over the wind farm area, (d) TKE profile 10–20 km downwind of the wind farm area, (e) potential temperature profile over the wind farm area, and (f) potential temperature profile 10–20 km downwind of the wind farm area. Horizontal dashed lines indicate the extent of the rotor area.

The turbulence profile associated with the LLJ also experiences impacts from the wind farm, as shown in Figs. 4c,d. When the wind farm is not present, TKE levels are very low all night, with a maximum value of 0.1 $m^2 s^{-2}$, except at 0600 LT, when a maximum value of 0.3 $m^2 s^{-2}$ occurs very near the ground, as the surface begins to warm. When the wind farm is included in the simulation, TKE within the wind farm (Fig. 4c) is increased greatly within the rotor area. The maximum value of TKE decreases over the night as the wind speeds decrease. Farther downwind (Fig. 4d), the TKE profiles are very similar to those without the wind farm, with the exception of a slightly elevated maximum above the top of the turbine rotor area. This feature is due to stronger advection of TKE at elevated levels where the wind speed is greater, and the dissipation of TKE is lower. The TKE at low levels is decreased slightly owing to the reduced wind shear in the wake. The overnight potential temperature profiles (Figs. 4e,f) within and downwind of the wind farm are only influenced slightly by the enhanced mixing induced in the rotor area; the steep temperature gradient located within the rotor area becomes slightly more smooth.

d. Evolution of the wake during the morning transition

The morning transition occurs between dawn (around 0600 LT) and 1000 LT, by which time the stable layer has completely eroded. During this transition time, the wake structure changes dramatically. Vertical profiles of the horizontal wind component averaged over the farm area between 0400 and 1200 LT on the second day are shown in Fig. 5a. Before dawn (0400–0600 LT), the LLJ within the rotor area is eliminated owing to energy extraction by the turbines, as discussed in the previous section. The wind deficit is at its greatest, and the wake persists far downwind at this time because there is inhibition of vertical mixing, and a lack of higher momentum flow aloft to be mixed downward. As the ground surface warms after 0600 LT (Fig. 5f), increased turbulent mixing reduces the wind shear within the rotor area. The wind deficit is smaller owing to reduced power production (as the wind speed is lower at this time), as well as increasing turbulence (Fig. 5d). By 1200 LT, the BL is well mixed and the wind profile steadily increases with height. Although power production is similar at this time to 0600 LT (Fig. 11), the wind deficit is small, at 0.4 m s^{-1} (a reduction of 6% at hub height), compared with 2.2 m s^{-1} (a reduction of 25%) at 0600 LT. The convective BL at 1200 LT allows efficient turbulent mixing of the momentum deficit within and above the rotor area, resulting in a smaller reduction of the wind.

Overnight and through the early morning, there is a large change in wind direction with height within the stable layer below 200 m (Fig. 5b). The wind is turned to the left of the geostrophic wind (which has a direction of 342° here) close to the surface due to Ekman turning. The enhanced mixing within the rotor area causes the u component of the wind to be reduced within the lower half of the rotor area and below, and increased in the upper half of the rotor area in the hours before dawn (Fig. 5c), owing to the background u-wind profile, which is a maximum at the bottom of the rotor area. At the same time, the v component of the wind is reduced within the rotor area, and increased below (Fig. 5e). The resulting change in the wind components leads to reduced Ekman turning in the lower half of the rotor area and down to the surface, with a maximum clockwise turning in the wind direction of 8° at the bottom tip of the rotor area before dawn. In the upper half of the rotor area, the Ekman turning is increased, with the wind direction turned anticlockwise by up to 4°. Above the rotor area to a height of around 300 m, the Ekman turning is again reduced. Above this height, there is minimal impact on the wind direction. During the day (1000 LT and later), after the stable layer has eroded and the BL is well mixed (Fig. 5f), there is little change in wind direction with height, and the wind farm has minimal impact. The wind within the rotor area turns more westerly after dawn. The reduction in Ekman turning causes divergence on the lhs of the wake (looking downwind), and convergence on the rhs. Where Ekman turning is increased, the opposite response occurs, with divergence on the rhs and convergence on the lhs. The divergence and convergence induces subsidence and uplift, respectively, and in turn, transports air with higher or lower momentum, depending on the wind profile at a particular height. The magnitude of Ekman turning varies with height, giving a complex wake structure when the BL is stably stratified. The convergence and divergence can also be described in terms of a gravity wave (discussed below).

The vertical structure of the wake during the morning transition is shown in Fig. 6. At 0530 LT before dawn (Fig. 6a), the momentum deficit within the rotor area is at its greatest, and the wake persists far downwind at hub height. Inhibition of vertical mixing within the stable layer, coupled with a lack of faster flow aloft to be mixed down (Fig. 5a), maximizes the wind reduction and the persistence of the wake. Above the leading edge of the farm, there is a column of decelerated flow, along with an accelerated column of flow at the rear, caused by uplift and subsidence, respectively. The momentum sink is mainly responsible for the convergence and associated uplift of the flow at the leading edge of the farm. The

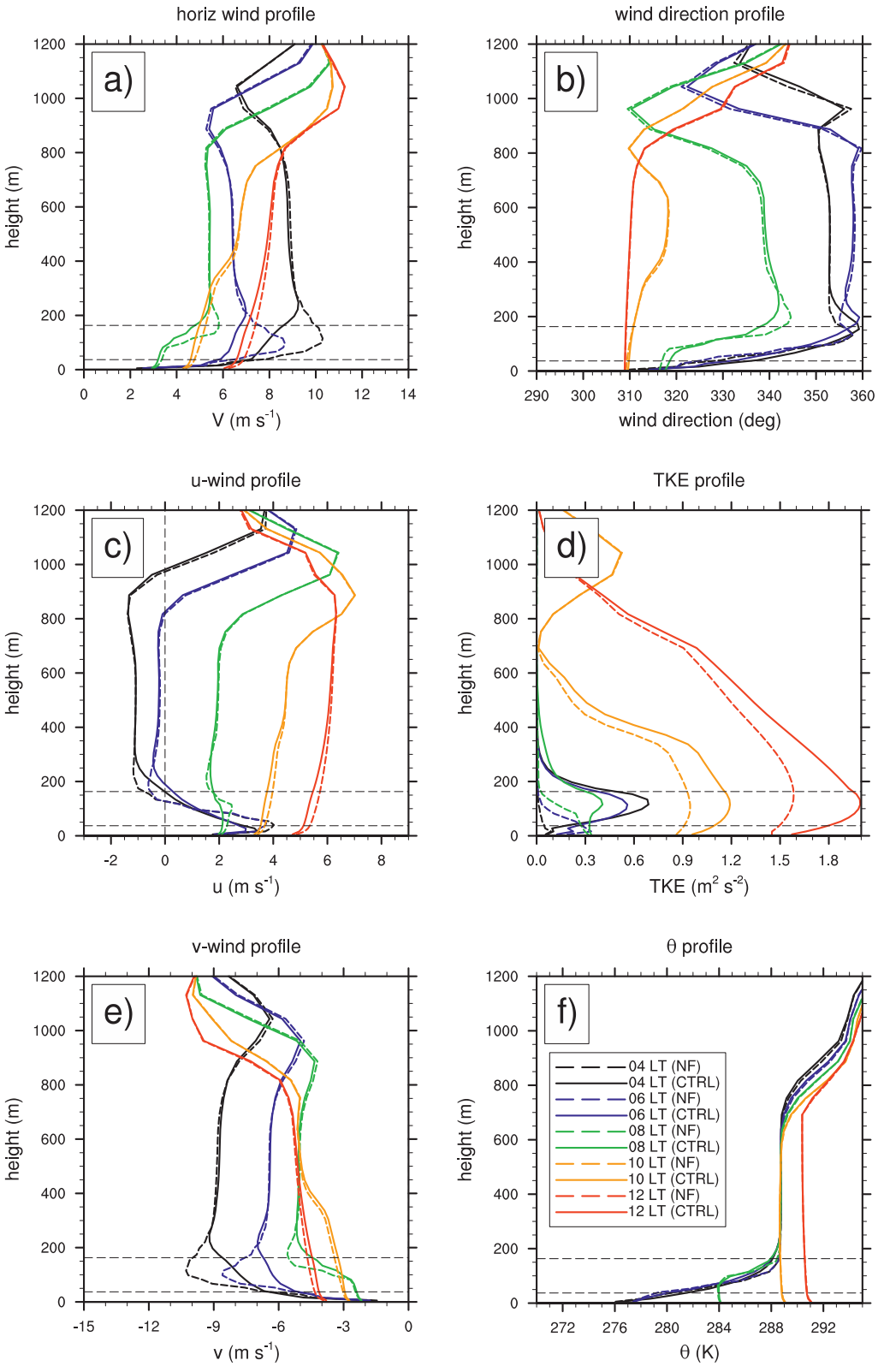

FIG. 5. Mean profiles over the wind farm area during the morning transition showing the wind farm (CTRL) and no-wind farm (NF) cases: (a) horizontal wind speed, (b) wind direction, (c) *u*-wind component, (d) TKE, (e) *v*-wind component, and (f) potential temperature. Horizontal dashed lines indicate the rotor area.

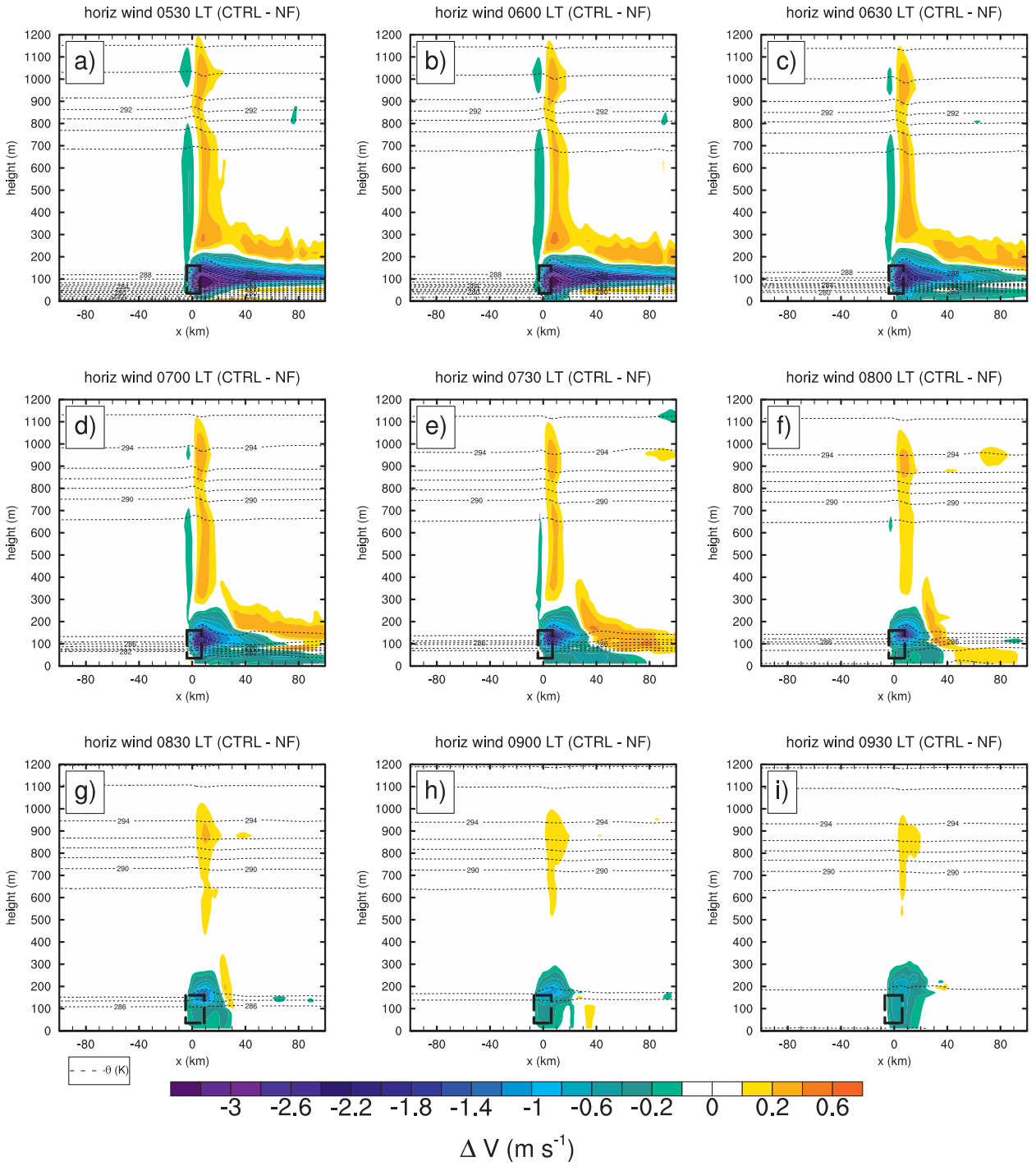

FIG. 6. Vertical structure of the wake during the morning transition, showing the horizontal wind speed difference between the wind farm (CTRL) and no-wind farm (NF) cases. Vertical cross sections taken along the dashed lines in Fig 7. Dashed rectangles indicate the rotor area.

source of TKE within the rotor area causes enhanced mixing of the LLJ within the rotor area (Fig. 5a), transporting higher momentum air to areas above and below the rotor area. The resulting accelerated flow is advected downwind and is apparent above the length of the wake. The divergent flow in the wake results in a small amount of subsidence aloft, transporting the accelerated flow downward. A reduction in the wind is not seen in the

wake below hub height in Figs. 6a,b, as Ekman turning advects the wake out of the cross section at 0530–0600 LT. At 0600 LT (Fig. 6b), the ground surface begins to warm and the stable layer is gradually eroded. At the same time, the wind weakens within the rotor area and above, and the LLJ decays. Power production reduces as a result, leading to a smaller reduction in the wind and the wake persisting gradually less far downwind over time (Figs. 6c–f).

By 0830 LT (Fig. 6g), the LLJ has nearly eroded away and the wind at hub height has reduced by nearly 6 m s^{-1} from 0530 LT. The power production and wind deficit are much reduced as a result. The greatest reduction in the wind occurs at the top of the rotor area, where a shallow stable layer still remains. As the LLJ has eroded, accelerated flow is no longer apparent above the wake. As time progresses, the stable layer is eroded completely, and the BL becomes convective and grows in depth. The enhanced turbulent mixing keeps the momentum deficit to a minimum, and the wake at hub height persists approximately 10 km downwind by 0930 LT (Fig. 6i). At this distance, the reduction in the wind is very small, at 0.1 m s^{-1} (2% relative to NF at hub height). As the morning progresses, winds accelerate and the wake becomes deeper and fills the depth of the BL (Fig. 3e).

The morning transition can also be understood by a plan view. In the horizontal, the wake exhibits the mean structure seen at night (Fig. 3b) until the ground surface begins to warm after 0600 LT (Figs. 7a,b). By 0630 LT, the wind within the rotor area has weakened and power production is reduced, leading to the wake decaying in strength and downwind extent (Fig. 7c). The accelerated flow aloft, generated by enhanced turbulent mixing of the LLJ within the rotor area to higher levels, continues to sink as the wake decays (Figs. 6c–f), and is eventually seen at hub height after 0630 LT. The accelerated flow first reaches hub height along the flanks of the wake and eventually replaces most of the downwind wake by 0730 LT. The arc-shaped features and splintering of the wake structure is a gravity wave response to the flow perturbation in the remaining stable layer interacting with the wind farm. We do not consider the exact spatial structure and orientation of this splintering to be robust, as slight deviations in stratification, coupled with inhomogeneities surrounding real wind farms, could greatly modify this gravity wave structure. However, the general descending of the accelerated flow throughout the morning transition period appears robust in Figs. 6 and 7.

e. Evolution of the wake during the evening transition

The evening transition takes place after around 1600 LT on the second day, when the ground surface begins to cool. Throughout the afternoon and evening, the wind at hub height accelerates, resulting in increasing power production and a greater deficit in the wind (Fig. 8a). The wind in the convective BL at 1400 LT is a maximum at the top of the BL, and there is little wind shear within the rotor area and above. As the ground surface continues to cool over time and the stable layer grows in depth (Fig. 8f), the wind shear within the rotor area increases. In addition, the wind within the rotor area and up to the top of the residual layer becomes supergeostrophic by 2000 LT. The wind is a maximum and roughly uniform with height from 200 to 800 m at 2000–2200 LT. By 2200 LT, the wind deficit has increased to 2.2 m s^{-1} (a reduction of 17% at hub height), from 0.5 m s^{-1} (a reduction of 6%) at 1400 LT. After 1600 LT, turbulence is mostly confined to the lower 300 m (Fig. 8d), inhibiting vertical mixing of faster air aloft into the momentum deficit.

From 1600 LT onward, as the ground surface cools, the wind direction begins to vary rapidly with height in the lower 300 m. The enhanced turbulent mixing from the wind farm modifies the u and v components of the wind (Figs. 8c,e) such that Ekman turning is reduced in the lower half of the rotor area and below, and increased above relative to NF to a height of around 300 m. The direction of the wind changes at most by a clockwise turning of 6° at the bottom tip of the rotor area, and an anticlockwise turning of 2° at the top of the rotor area at 2200 LT (Fig. 8b).

The evolution of the wake in the horizontal during the evening transition is shown in Figs. 9a–c. The wake grows over time, in both strength and persistence downwind, owing to increasing power production and inhibition of vertical mixing within the growing stable layer. A small region of weakly accelerated flow develops on the lhs of the wake (facing downwind) in conjunction with the growth of the stable layer and increase in wind shear within the rotor area. As discussed previously, the increased turbulent mixing within the wind farm causes the wind to turn clockwise in the lower half of the rotor area and below, and to a lesser degree, anticlockwise in the upper half of the rotor area and above (Fig. 8b). The clockwise turning of the wind within the farm causes divergence on the lhs of the farm and wake, and convergence on the rhs (with respect to the incoming flow). In turn, there is subsidence on the lhs, and uplift on the rhs, which results in faster air aloft being advected down on the lhs, and slower air advected up on the rhs. The greatest acceleration is seen at the level of the bottom tip of the rotor area, up to 0.7 m s^{-1} (an increase of 7% relative to NF) at 2000 LT, where the clockwise turning of the wind and divergence is greatest. The response to the Ekman turning causes the maximum

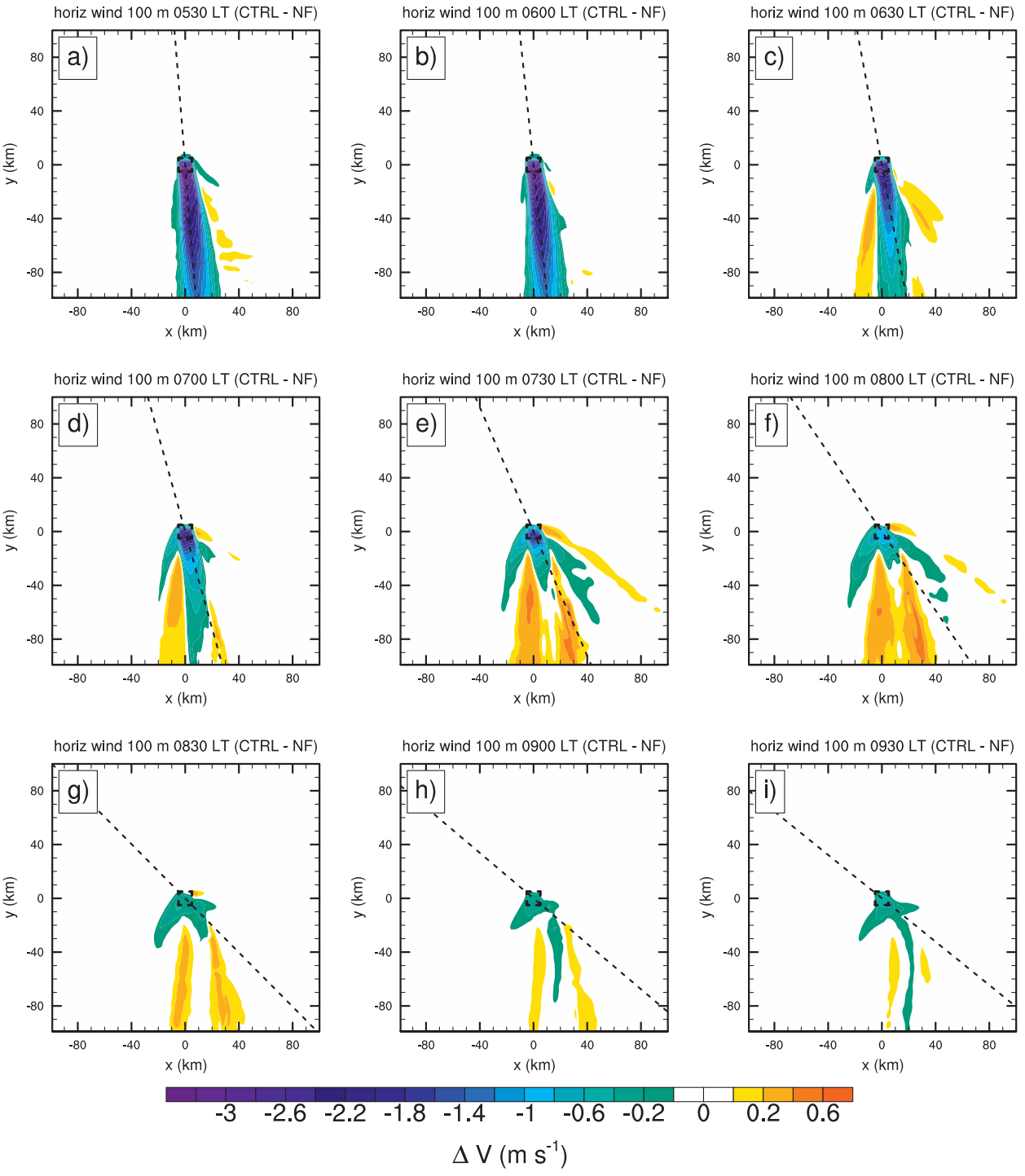

FIG. 7. Horizontal structure of the wake during the morning transition, showing the horizontal wind speed difference between the wind farm (CTRL) and no-wind farm (NF) cases. Dashed squares indicate the wind farm area; straight dashed lines indicate the direction of the incoming northwesterly flow.

wind deficit to shift slightly toward the rhs of the wake at this time.

In the vertical, the wake occupies a shallower depth over time (Figs. 9d–f), as the stable layer grows and inhibits vertical mixing. As the magnitude of the wind speed deficit grows during the evening transition, the increased shear in the lowest 100 m is reduced with respect to NF from the extraction of momentum.

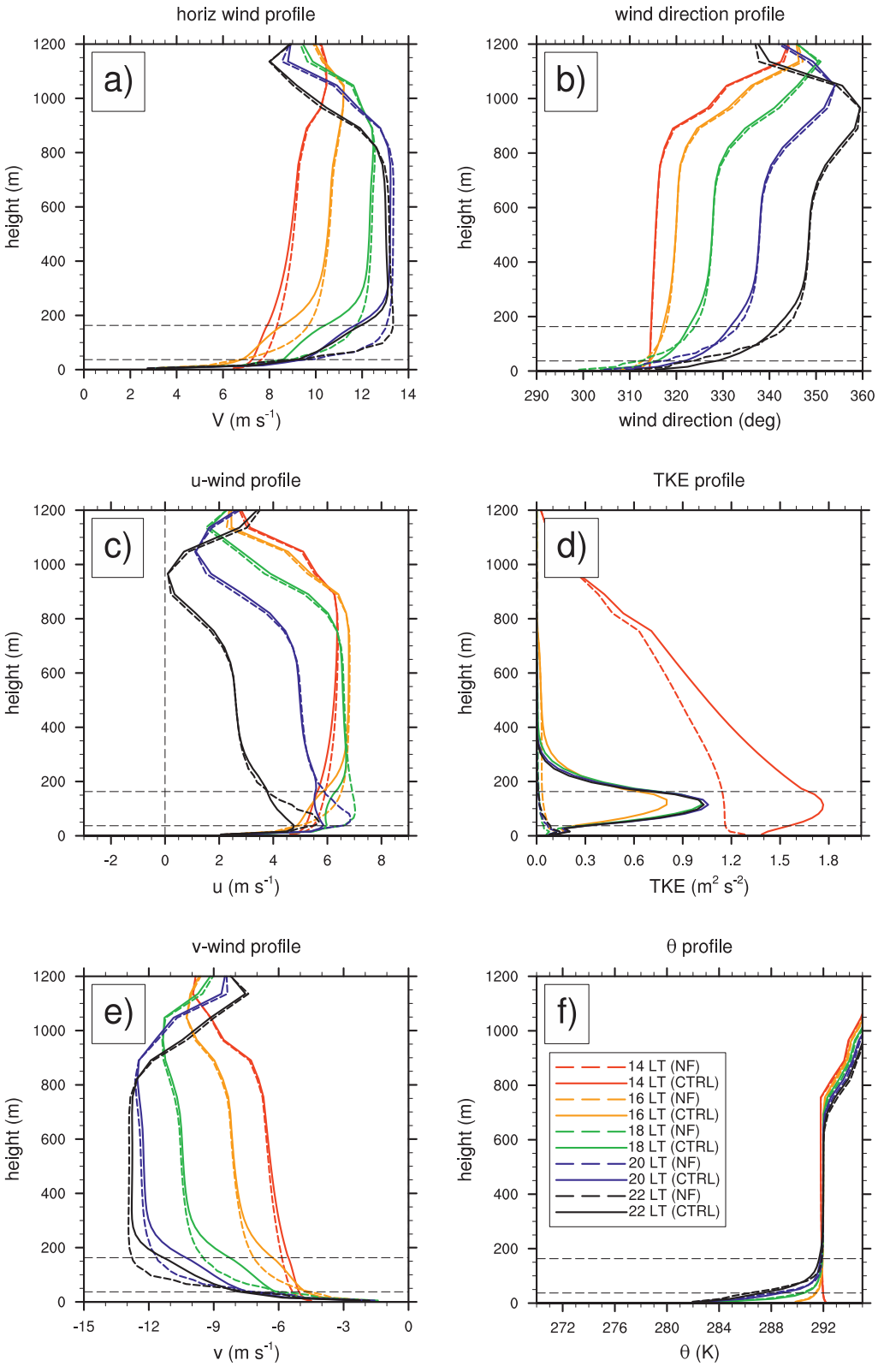

FIG. 8. Mean profiles over the wind farm area during the evening transition showing the wind farm (CTRL) and no-wind farm (NF) cases: (a) horizontal wind component, (b) wind direction, (c) *u*-wind component, (d) TKE, (e) *v*-wind component, and (f) potential temperature. Horizontal dashed lines indicate the rotor area.

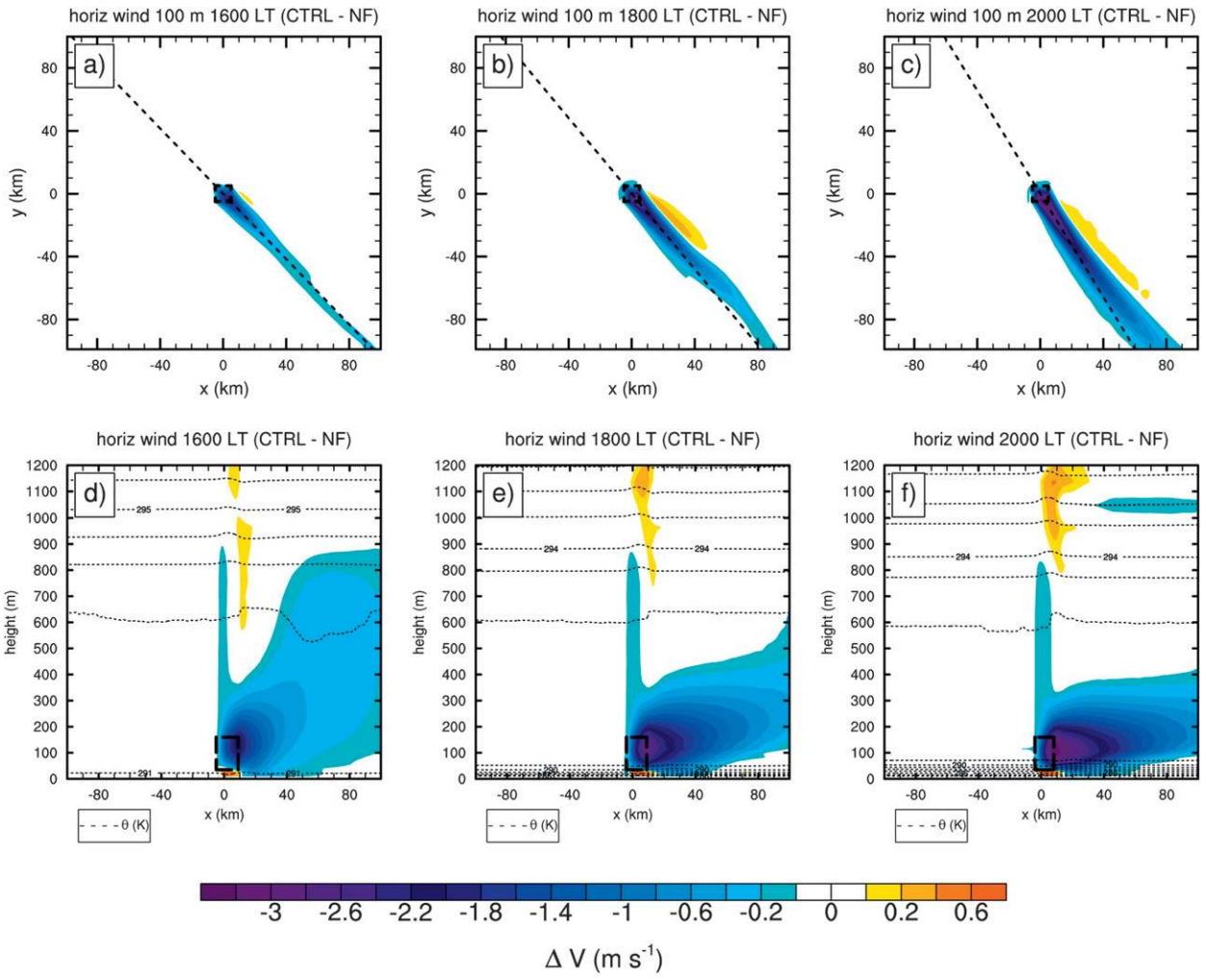

FIG. 9. Structure of the wake during the evening transition, showing the horizontal wind speed difference between the wind farm (CTRL) and no-wind farm (NF) cases: (a)–(c) horizontal cross sections at hub height (100 m) and (d)–(f) vertical cross sections along the dashed lines in (a)–(c). Thin dashed lines indicate potential temperature in CTRL; thick dashed rectangles indicate the wind farm area; straight dashed lines indicate the direction of the incoming northwesterly flow.

f. Wind farm influence on temperatures and heat fluxes

The wind farm induces a temperature perturbation within the atmosphere, both above and below the rotor area, as well as downwind. The temperature difference between the CTRL and NF cases over the wind farm area is shown in Fig. 10a. During the night and through the morning transition, warming occurs in the lower half of the rotor area and below to the surface, and cooling occurs in the upper half of the rotor area and above to a height of 200–250 m. This smoothing of the temperature gradient in the stable layer is also shown in Fig. 4e. The greatest warming is seen at the bottom tip of the rotor area in the hours before dawn, with a maximum of 1.1 K at 0300 LT on the second day. Near the surface, the amount of warming is smaller, with a maximum increase of 0.5 K at 2 m above the ground at 1900 LT on the second day (Fig. 10c). The cooling in the upper half of the rotor area reaches a maximum of 0.8 K around dawn on the second day. The maximum temperature perturbation occurs when the stable layer is deepest and most strongly stratified, along with the greatest increase of TKE from shear generation and parameterized source from the turbines, resulting in increased turbulent mixing of higher θ air down and lower θ air upward. During the day, little temperature change occurs, as the dynamics of the well-mixed BL overwhelm the perturbation from the wind farm. The mean temperature change over the wind farm area at 2 m during the simulation period is +0.2 K, a slight warming.

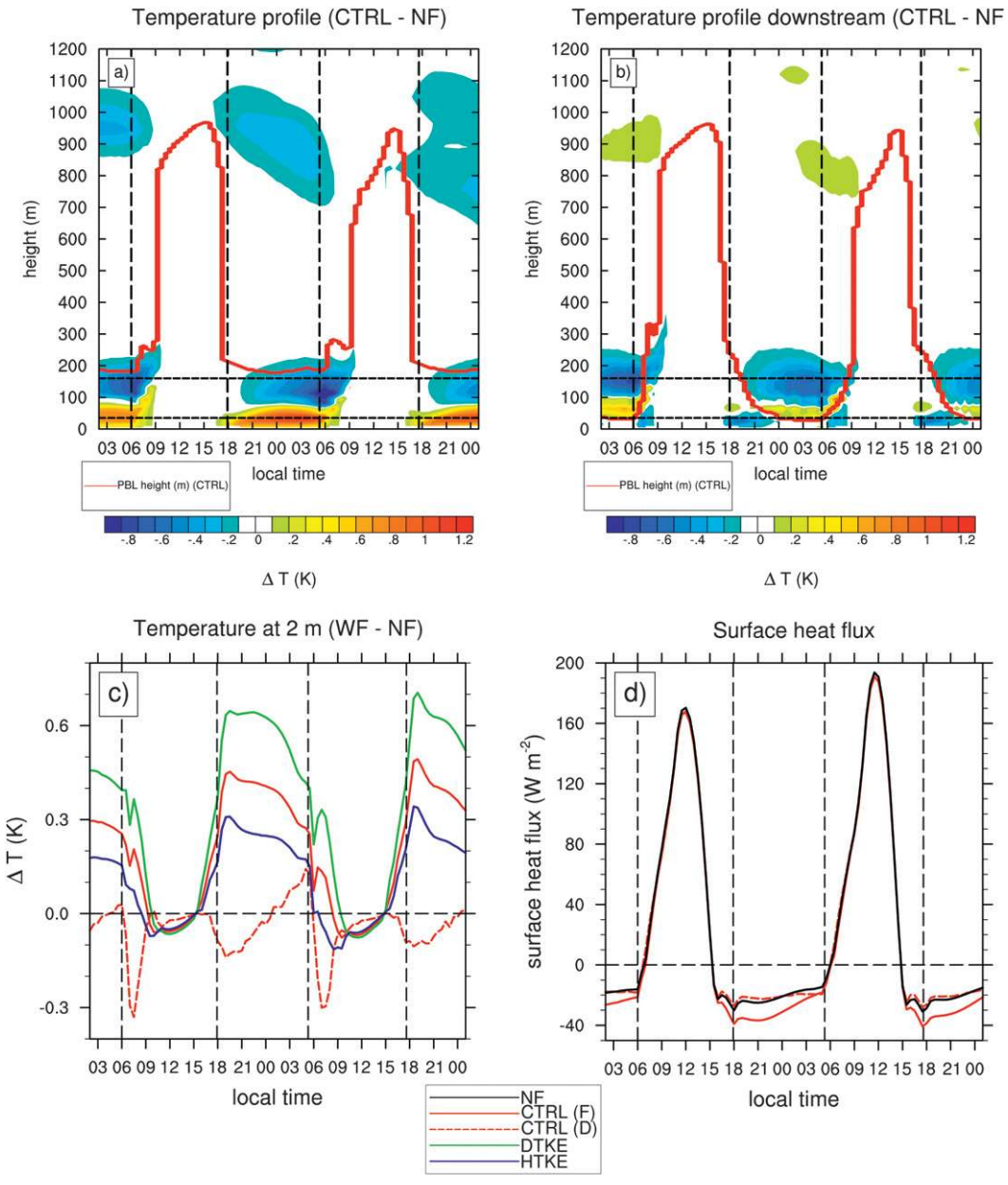

FIG. 10. Evolution of the mean profile of temperature difference between the wind farm (CTRL) and no-wind farm (NF) cases: (a) over the wind farm area and (b) 10–20 km downwind. (c) Evolution of the near-surface temperature change at 2 m. (d) Evolution of the surface heat flux in the no-wind farm case (NF), and over the wind farm [CTRL (F)] and downwind [CTRL (D)]. Vertical dashed lines indicate sunrise and sunset times; horizontal lines in (a) and (b) indicate the extent of the rotor area.

A subtle cooling is seen within the inversion above the residual layer (700–1100 m AGL) over the farm (Fig. 10a) during the night, when air flowing over the wind farm is forced upward, resulting in adiabatic cooling. The counterpart downward motion in this gravity wave has a small impact downwind of the wind farm (Fig. 10b), where a weak warming of 0.1 K appears in the stable inversion overlying the residual layer during the morning transition periods.

The surface temperature perturbation 10–20 km downwind of the wind farm is much smaller (Fig. 10b) than that within the wind farm. The greatest change downwind occurs above the surface within the rotor area, with cooling in the upper half of the rotor area, and warming in the lower half. The maximum cooling is by 0.7 K at the upper tip of the rotor area at 0600 LT on the first day, with a warming by the same amount in the

lower half of the rotor area. Cooling occurs close to the ground during the morning and evening transitions, with a maximum cooling of around 0.3 K at a height of 2 m at 0730 LT on the first day (Fig. 10c). These temperature perturbations are much smaller downwind because the TKE has been strongly dissipated, and with a weakened LLJ, there is much less low-level wind shear for TKE production. The mean near-surface temperature change downwind of the wind farm during the entire simulation is negligible, at −0.05 K.

The small change in the near-surface temperature induces a change in the surface heat flux at night (Fig. 10d), while negligible change in the surface heat flux is seen during the day, either within the farm or downwind. As the ground surface begins to cool, and the stable layer forms, a small increase in temperature occurs near the ground (Fig. 10c). The extra near-surface warmth results in more heat being lost to the ground, with a small increase seen in the negative surface heat flux (Fig. 10d). There is a maximum increase in the negative heat flux of 12 W m^{-2} between 1930 and 2200 LT on the first day. During the daytime, there is a decrease in the positive heat flux of 1–3 W m^{-2} at most. Downwind, the change in surface heat flux is smaller. The larger heat fluxes at night may be influenced by the prescribed skin temperatures, as the changes in the 2-m temperatures due to turbulent mixing could impact the skin temperatures. However, this would likely act to warm the skin temperatures, creating a negative feedback, which would reduce the magnitude of the surface fluxes. This suggests the increased negative surface heat fluxes in the GABLS2 simulation provide an upper bound in values, and that the impact of the wind farm on the surface fluxes is likely less. Future studies will need to be performed using fully coupled land surface models to investigate whether any other feedbacks become exposed with more physically comprehensive experiments. However, owing to the small temperature perturbations and short time periods involved, these feedbacks are expected to be slight.

The changes in temperature and heat fluxes are caused primarily by enhanced turbulent mixing within the rotor area. The majority of the increase in TKE within the farm is from that directly produced by the wind farm parameterization, and is the greatest source of uncertainty. To assess the uncertainty associated with the magnitude of the temperature perturbation, we performed two additional simulations. In one simulation (denoted DTKE), the source of TKE added by the parameterization was doubled, and in the other (denoted HTKE), the source of TKE was reduced by half. When the source of TKE was doubled, the maximum change in temperature at 2 m increased to 0.7 K at 1900 LT on the second day, an increase of 0.2 K relative to CTRL. Downwind, the maximum change in temperature is unchanged. The mean temperature change over the farm during the simulation period is increased slightly to 0.3 K. When the source of TKE was halved, the maximum temperature change at 2 m was 0.3 K, with a mean temperature increase of 0.1 K; a small reduction relative to CTRL. The amount of TKE directly added in the rotor area represents the energy extracted by the turbines that is not converted into useful energy. Doubling or halving the TKE source represents an extreme range in values that will most likely not be seen in reality if turbine mechanical/electrical losses are approximately 10%. Therefore, these experiments provide upper bounds to the uncertainty in this component of the parameterization.

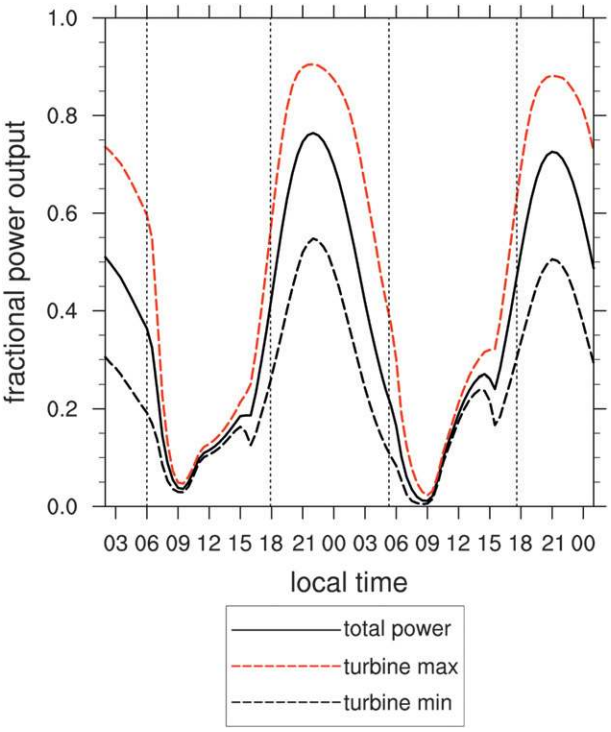

FIG. 11. Evolution of power output, as a fraction of the theoretical maximum. The black solid line indicates the total power output of the wind farm; the red dashed line indicates the power output of the most productive turbine upwind; the black dashed line indicates the power output of the least productive turbine downwind. Vertical dashed lines indicate sunrise and sunset times.

g. *Power output*

The power collection by the entire wind farm varies as a function of both the inflow wind speed, and the magnitude of the wake deficit, which varies with atmospheric stability as discussed earlier. The total power output of the wind farm over the simulation period, as a fraction of the theoretical maximum output, is shown in Fig. 11. The power output was calculated for each grid cell containing

wind turbines using the power coefficient as the fraction of energy extracted from the atmosphere that is converted into useful energy by the turbines, according to Eq. (11) in Fitch et al. (2012). The theoretical maximum power output is the power output if all the turbines were operating at their nominal rated power output (i.e., 5 MW for each turbine).

The wind farm produces the most power during the night, when the wind speed in the rotor area is greater, despite the fact that the wake deficit is large during this time. During the first night, the mean fractional power output is 0.56, more than a factor of 3 greater than during the day, when the mean fractional power output is 0.17. The maximum fractional power output of the wind farm is 0.76 at 2200 LT on the first day, when the wind speed within the rotor area is greatest. The power output falls to a minimum of 0.01 at 0900 LT on the second day, when the wind speed is lowest. The evolution of the power output follows that of the wind speed, as discussed in section 3a.

Within the wind farm, there is a considerable degree of variability in the power output of individual turbines, depending on the influence of atmospheric stability in mixing out the wake. During the daytime, after the morning transition, but before the ground begins to cool in the afternoon (around 1500 LT), there is a relatively small difference between the maximum power output of a single turbine (located at the upwind edge of the farm) and the minimum power output of one turbine (located at the downwind edge) (Fig. 11). While the power output of the farm as a whole is low at this time, reducing the momentum needed to replenish the deficit, the more efficient turbulent mixing in the daytime convective BL also keeps the momentum deficit at downwind turbines to a minimum. Between 1100 and 1430 LT on the first day, the least productive turbine produces at least 80% of the power of the most productive turbine upwind. Once the stable layer begins to form around 1600 LT, the difference in power output grows between upwind and downwind turbines. The upwind turbines produce more power, and more momentum is required to replenish the deficit, while vertical mixing is inhibited in the growing stable layer. The difference in power output between turbines continues to increase during the night, when at 0600 LT on the second day, the least productive turbine produces 28% of the power of the most productive turbine. By 0000 LT, the growth of an LLJ within the rotor area and the deceleration of flow aloft reduce the exchange of momentum, maximizing the wind deficit downwind.

The power output over time of individual turbines as a fraction of the theoretical maximum for one turbine is shown in Fig. 12. Turbines at the upwind (northwest) edges of the farm produce the most power, with the turbines at the upwind corners typically the most productive, as these locations are most exposed to the incoming flow. The least productive turbines are located at the downwind edges of the farm, farthest from the most productive turbines along the direction of flow. The pressure gradient is more favorable at the upwind corners, and for this case, along the lhs of the wake (looking downwind) compared with the rhs of the wake at night, leading to greater power output in these locations. This pressure gradient is associated with the convergence and divergence pattern from the impact of the farm on Ekman turning (discussed in section 3d); in other terms, a gravity wave. During the day, the pressure gradient is more uniform over the farm (not shown), and there is less variation in power output.

To assess the impact of the magnitude of the TKE source on power production, the power output of the DTKE and HTKE experiments (discussed in section 3f) was compared to CTRL. A very small difference in the power output was found, with downwind turbines producing slightly more power in the DTKE experiment, due to enhanced mixing caused by higher TKE (figure not shown).

4. Discussion and conclusions

We explored the interaction between a large onshore wind farm and the BL throughout a diurnal cycle by assessing the impact on local and mesoscale flow, turbulence, temperature, surface heat flux, and power output. We employed a new wind farm parameterization for WRF (Fitch et al. 2012), which is distributed in WRF v3.3 and later, to represent the effects of a wind farm. Wind turbines are modeled by imposing a momentum sink on the mean flow at model levels within the rotor area. Kinetic energy (KE) is transformed into electricity and turbulent kinetic energy (TKE), with the fraction of KE extracted from the atmosphere quantified by the thrust coefficient of a modern commercial turbine. The fraction of KE extracted, which is not transformed into electricity, generates TKE.

We performed simulations using initial and boundary conditions provided by the well-studied GABLS2 case (Svensson et al. 2011), which simulates a strong diurnal cycle in a region of the U.S. Midwest in Kansas, an area experiencing tremendous wind farm development. The presence of a wind farm covering 10 km $\times$ 10 km, with 100 turbines of nominal power output of 5 MW, is found to have a significant impact, not only on the local atmospheric flow, but also at distances of up to 60 km downwind at night. The magnitude of the impact and the structure of the wake differ greatly between daytime and

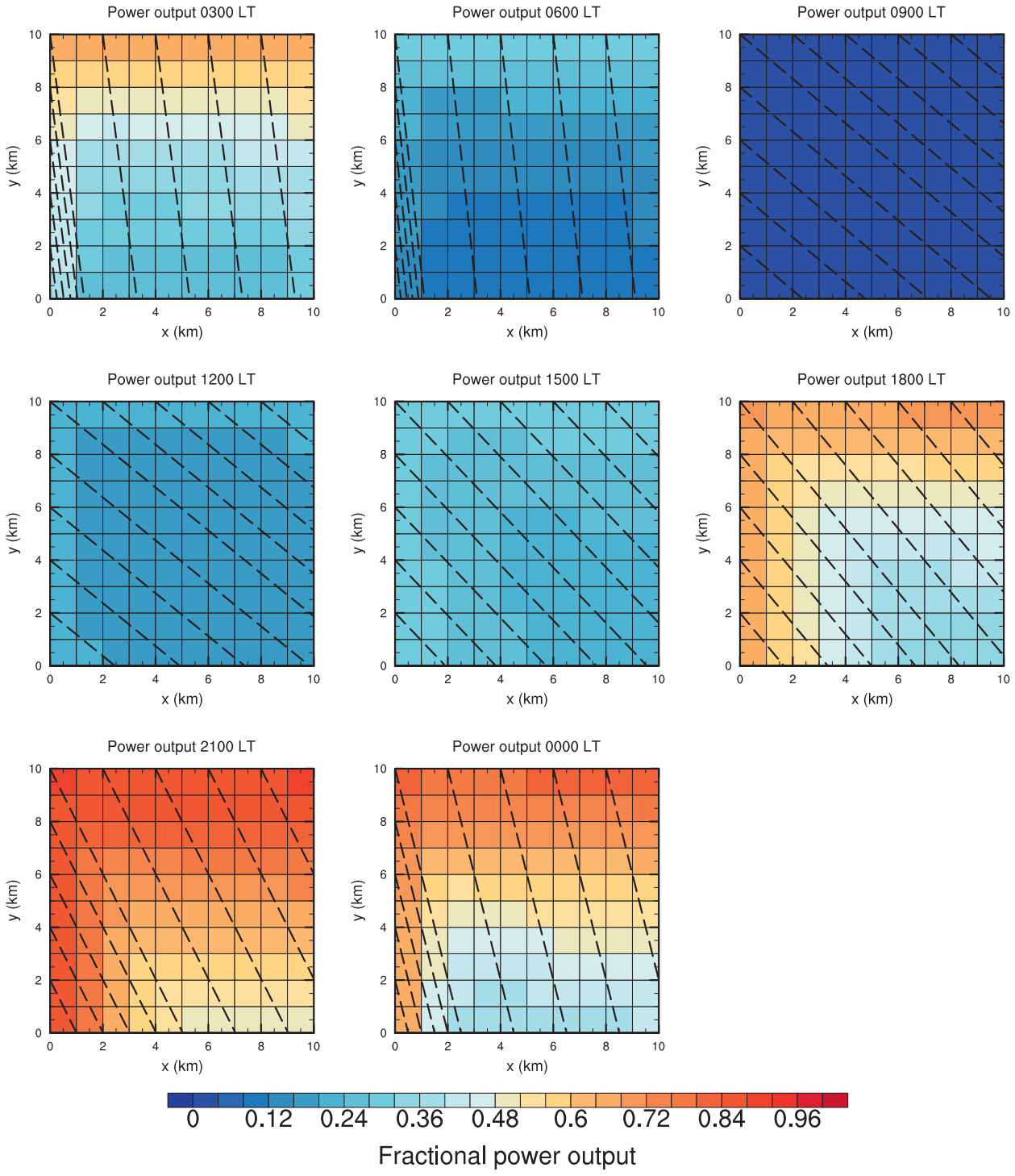

FIG. 12. Evolution of the power output for each turbine, as a fraction of the theoretical maximum. Dashed lines indicate the direction of the incoming northwesterly flow.

nighttime; a rapid evolution between the two regimes occurs during the morning and evening transitions. A smaller amount of energy is extracted by the turbines during the day, owing to the weaker wind, which leads to a smaller momentum deficit. The stability of the BL also has a great impact on the length and structure of the wake. During the day, the unstable stratification gives rise to more vigorous vertical mixing, which leads to the

momentum deficit being spread throughout the depth of the BL. A smaller reduction in the wind occurs as a result. Conversely at night, the stable layer within the rotor area inhibits turbulent mixing of the momentum deficit, leading to a shallower wake and a greater reduction in the wind. A maximum reduction of 10% in the wind at hub height occurs at the downwind edge of the farm during the day, which increased by a factor of 3 at night, to 30%. The wake has an *e*-folding distance of 15 km during the day at hub height, which increases by a factor of nearly 4, to 55 km at night. A 10% deficit in the wind persists for 60 km downwind at hub height during the night. These distances likely indicate upper bounds in values, as the domain considered is uniform. In reality, mesoscale conditions downwind are likely to vary, and together with impacts of terrain, could act to dissipate the wake downwind. An LLJ forms within the rotor area in the hours before dawn, and is completely eliminated above the wind farm due to the extraction of momentum by the turbines. The lack of faster flow aloft to be mixed down, in addition to inhibition of vertical mixing, leads to a maximum in the wind speed reduction at this time.

In addition to influencing wind profiles, the wind farm significantly influences TKE, turbulent mixing, and boundary layer height. TKE is produced directly by the parameterization, representing the energy extracted by the turbines that does not produce electricity. The parameterized momentum sink also enhances the wind shear, which produces additional TKE. During the day, the wind farm causes an increase of TKE throughout the depth of the BL, with a maximum increase of 33% in the upper half of the rotor area. At night, the relative increase in TKE is much greater, as ambient turbulence is low and energy production is greater. Within the rotor area, TKE increases by a factor of 20 at night. An increase also occurs above the rotor area, to a height of around 250 m. The enhanced turbulent mixing within the rotor area leads to an increase in the height of the BL above the farm at night by up to 145 m; an increase by a factor of more than 4. During the day, the change in BL height caused by the wind farm is negligible.

Within the stable layer at night, there is a large change in wind direction with height (the Ekman spiral). The enhanced turbulent mixing within the rotor area changes the u and v components of the wind, such that Ekman turning is reduced in the lower half of the rotor area and below, and increased above to a height of around 300 m, when the wind shear is positive at all levels in the BL (before the LLJ develops). The wind turns clockwise by up to 8° at the bottom tip of the rotor area, and anticlockwise by up to 4° at the top of the rotor area. The clockwise turning of the wind within the lower half of the rotor area causes divergence on the lhs (with respect to the incoming flow) of the farm and wake, and convergence on the rhs. In turn, subsidence, advecting faster flow to lower levels results on the lhs, and uplift, advecting slower air upward, on the rhs. The maximum wind deficit is seen slightly to the rhs of the wake, as a result. On the lhs, the deficit is reduced slightly, and at the bottom of the rotor area, there is a small increase in the wind, of up to 0.7 m s^{-1} (7%). The accelerated flow also occurs downstream on the lhs of the wake. Once the LLJ develops, the wind profile becomes more complex, and in turn, so does the impact of Ekman turning on the wake structure.

Close to the ground, at a height of 10 m, a maximum reduction in the wind of 6% is seen during the day. However, at night, the wind accelerates beneath the rotor area, by up to 19%, similar to the accelerations under the rotor disks seen by Rajewski et al. (2013). The increased TKE within the rotor area causes enhanced turbulent mixing of faster flow to lower levels. The convergence and divergence circulation discussed above gives rise to an acceleration on the lhs of the wake downwind. Deceleration occurs on the rhs of the wake, with a reduction in the wind of up to 11%.

The wind farm induces a temperature and heat flux perturbation both within and downwind of the wind farm. The maximum temperature perturbation occurs in the hours before dawn, when the stable layer is deepest and most strongly stratified, and experiences a large increase of TKE within the rotor area. The temperature perturbation results from the increased turbulent mixing within the rotor area mixing higher θ air down, and lower θ air upward, in a similar fashion to Baidya Roy et al. (2004) and Baidya Roy and Traiteur (2010). During the day, little temperature change occurs owing to the well-mixed BL dominating the impact of the wind farm. At night, warming occurs in the lower half of the rotor area and below to the surface, and cooling occurs in the upper half of the rotor area and above to a height of 200–250 m. A maximum warming of 1 K occurs at the bottom of the rotor area; however, near the surface, the amount of warming is smaller, by up to 0.5 K. The cooling in the upper half of the rotor area reaches a maximum of 0.8 K. The change in temperature within the rotor area is similar to that seen in LES by Lu and Porté-Agel (2011). Downwind, the surface temperature perturbation is small, with a cooling of up to 0.3 K. Over the simulation period, the mean temperature change over the wind farm area at 2 m is +0.2 K, a very slight warming. The mean temperature change downwind is negligible. The change in near-surface temperature induces a small change in the surface heat flux at night, with the downward flux increasing by up to 12 W m^{-2}. During the day, and downwind at all times, the change in surface heat flux is negligible.

Future work should include more complete land surface physics to address any sensitivities that may exist with soil temperature changes caused by the temperature perturbation induced by the wind farm, but as discussed in section 3f, this feedback is likely small and is outside the scope of this study.

Total wind farm power production for the GABLS case is more than a factor of 3 greater at night than during the day, when the wind in the rotor area is strongest. The mean total power output of the wind farm as a fraction of the theoretical maximum is 0.56 at night, compared with 0.17 during the day. The maximum fractional power output of the farm reaches 0.76 during the night. Within the wind farm, there is a considerable degree of variability in the power output of individual turbines. During the day, when less energy is extracted by the turbines, the difference in power output between upwind and downwind turbines is relatively small, with downwind turbines producing at least 80% of the power of upwind turbines. In addition to the amount of energy extracted by upwind turbines, atmospheric stability has a great impact on the power output of downwind turbines. In the unstable BL during the day, strong turbulent mixing constrains the momentum deficit at downwind turbines to a minimum. In contrast, once the stable layer begins to grow, the difference in power output between upwind and downwind turbines widens due to a combination of suppressed vertical mixing and greater extraction of kinetic energy from the faster flow by upwind turbines. As the stable layer deepens throughout the night, the difference in power output increases, with downwind turbines producing a minimum of 28% of the power of upwind turbines. Schepers et al. (2012) observed maximum power deficits of 80% 3.5 rotor diameters downwind of a single line of 5 turbines during nocturnal conditions with very low ambient turbulence intensity.

The impact of the magnitude of the TKE produced by the parameterization is assessed, with experiments doubling and halving the amount of TKE produced. When the source of TKE is doubled, the maximum change in temperature at 2 m increases by 0.2 K, to 0.7 K. Downwind, the maximum change in temperature is unchanged. The mean temperature change over the farm during the simulation period is increased slightly to 0.3 K. When the source of TKE is halved, the maximum temperature change at 2 m is reduced to 0.3 K, while the mean temperature change decreases slightly to 0.1 K. The sensitivity of power production to the TKE source is found to be very small, with downwind turbines producing slightly more power with higher TKE. Although the source of TKE is likely overestimated, as mechanical/electrical losses are neglected (which should consume some of the energy extracted by the turbines), the overestimate is likely to be small, as estimates of turbine mechanical/electrical losses are around 10%. Doubling or halving the TKE source represents an extreme range in values that will not likely be seen in practice.

Some caution should be used in interpreting the power output of individual turbines. The detailed wake structure from each turbine is not resolved; therefore, the precise flow characteristics at downwind turbines will not be captured, which could influence the power output for a specific turbine. The wind deficit calculated is the average over one grid box, which in this case has a length of 1 km in the horizontal. Furthermore, in this idealized study, there is no mechanism to cause the wake to meander in the horizontal or vertical. Future studies with simulation codes capable of resolving individual turbines and large eddies, exploring real case studies with complex terrain, are needed to elucidate the wake structures of individual turbines and their impact on the power output of downwind turbines.

There are few observations available to verify the results presented in this study. Christiansen and Hasager (2005) have quantified the wind speed deficit in the wake of an offshore wind farm for near-neutral and unstable conditions using synthetic aperture radar. Their observations agreed well with results using the wind farm parameterization employed here for an offshore case (Fitch et al. 2012). However, the difference in surface roughness between offshore and onshore cases will have a considerable impact on the wake, in addition to the stability (Churchfield et al. 2012). Field experiments, such as those discussed by Rajewski et al. (2013) will be needed to verify the results presented here, and to further develop models of wind farm induced flow.

Fitch et al. (2012) found the wind farm parameterization employed in the present work agreed well with previous LES studies. Regions of enhanced TKE and momentum fluxes agreed well with the LES reported by Lu and Porté-Agel (2011), and with wind tunnel experiments reported by Chamorro and Porté-Agel (2009). In addition, the enhancement of eddy diffusivity associated with turbine mixing is similar to the LES reported by both Calaf et al. (2010) and Lu and Porté-Agel (2011).

In the future, studies exploring the impact of a wide range of surface roughness throughout a diurnal cycle would be illuminating. Churchfield et al. (2012) found a significant impact on the power output of downwind turbines with different surface roughness. However, their simulations studied two wind turbines in LES. It would be valuable to explore the impact within a large wind farm containing numerous turbines.

The wake studied here is found to persist for great distances downwind during the night, when the ambient wind is strong and the conditions are stable. A 10%

reduction in the wind persists 60 km downwind from the farm at hub height. These distances are even greater than the typical gridbox size employed in coarse-resolution NWP. With increasingly large wind farms in development, the impact on atmospheric flow in NWP may need to be considered. The parameterization employed in this study is efficient, with relatively little sensitivity to vertical and horizontal resolution, and thus, could be used in operational NWP.

Acknowledgments. We wish to thank REpower for providing the thrust and power coefficients for the 5M turbine. We express our appreciation for research funding from a variety of sources. Funding for ACF is from NORCOWE, and support for JKL is from NREL LDRD 06501101. We thank Jimy Dudhia for useful discussions. All the simulations were performed on the NREL/Sandia Red Mesa high-performance computing system. NREL is a national laboratory of the U.S. Department of Energy, Office of Energy Efficiency and Renewable Energy, operated by the Alliance for Sustainable Energy, LLC.

REFERENCES

Adams, A. S., and D. W. Keith, 2007: Wind energy and climate: Modeling the atmospheric impacts of wind energy turbines. *Eos, Trans. Amer. Geophys. Union,* **88** (Fall Meeting Suppl.), Abstract B44B-08.

Baidya Roy, S., 2011: Simulating impacts of wind farms on local hydrometeorology. *J. Wind Eng. Ind. Aerodyn.,* **99,** 491–498, doi:10.1016/j.jweia.2010.12.013.

——, and J. J. Traiteur, 2010: Impacts of wind farms on surface air temperatures. *Proc. Natl. Acad. Sci. USA,* **107,** 17 899–17 904.

——, S. W. Pacala, and R. L. Walko, 2004: Can large wind farms affect local meteorology? *J. Geophys. Res.,* **109,** D19101, doi:10.1029/2004JD004763.

Banta, R. M., Y. L. Pichugina, and R. K. Newsom, 2003: Relationship between low-level jet properties and turbulence kinetic energy in the nocturnal stable boundary layer. *J. Atmos. Sci.,* **60,** 2549–2555.

Barrie, D. B., and D. B. Kirk-Davidoff, 2010: Weather response to a large wind turbine array. *Atmos. Chem. Phys.,* **10,** 769–775, doi:10.5194/acp-10-769-2010.

Barthelmie, R. J., and L. E. Jensen, 2010: Evaluation of wind farm efficiency and wind turbine wakes at the Nysted offshore wind farm. *Wind Energy,* **13,** 573586, doi:10.1002/we.408.

Blahak, U., B. Goretzki, and J. Meis, 2010: A simple parameterization of drag forces induced by large wind farms for numerical weather prediction models. *Proc. European Wind Energy Conf. and Exhibition 2010,* Warsaw, Poland, European Wind Energy Association, 186–189.

Cal, R. B., J. Lebrón, L. Castillo, H. S. Kang, and C. Meneveau, 2011: Experimental study of the horizontally averaged flow structure in a model wind-turbine array boundary layer. *J. Renewable Sustainable Energy,* **2,** 013106, doi:10.1063/1.3289735.

Calaf, M., C. Meneveau, and J. Meyers, 2010: Large eddy simulation study of fully developed wind-turbine array boundary layers. *Phys. Fluids,* **22,** 015110, doi:10.1063/1.3291077.

——, M. B. Parlange, and C. Meneveau, 2011: Large eddy simulation study of scalar transport in fully developed wind-turbine array boundary layers. *Phys. Fluids,* **23,** 126603, doi:10.1063/1.3663376.

Chamorro, L. P., and F. Porté-Agel, 2009: A wind-tunnel investigation of wind-turbine wakes: Boundary-layer turbulence effects. *Bound.-Layer Meteor.,* **132,** 129–149, doi:10.1007/s10546-009-9380-8.

Christiansen, M. B., and C. B. Hasager, 2005: Wake effects of large offshore wind farms identified from satellite SAR. *Remote Sens. Environ.,* **98,** 251–268, doi:10.1016/j.rse.2005.07.009.

Churchfield, M. J., S. Lee, J. Michalakes, and P. J. Moriarty, 2012: A numerical study of the effects of atmospheric and wake turbulence on wind turbine dynamics. *J. Turbul.,* **13,** 1–32, doi:10.1080/14685248.2012.668191.

Fiedler, B. H., and M. S. Bukovsky, 2011: The effect of a giant wind farm on precipitation in a regional climate model. *Environ. Res. Lett.,* **6,** 045101, doi:10.1088/1748-9326/6/4/045101.

Fitch, A. C., J. B. Olson, J. K. Lundquist, J. Dudhia, A. K. Gupta, J. Michalakes, and I. Barstad, 2012: Local and mesoscale impacts of wind farms as parameterized in a mesoscale NWP model. *Mon. Wea. Rev.,* **140,** 3017–3038.

Hansen, K. S., R. J. Barthelmie, L. E. Jensen, and A. Sommer, 2012: The impact of turbulence intensity and atmospheric stability on power deficits due to wind turbine wakes at Horns Rev wind farm. *Wind Energy,* **15,** 183–196, doi:10.1002/we.512.

Högström, U., D. N. Asimakopoulos, H. Kambezidis, C. G. Helmis, and A. Smedman, 1988: A field study of the wake behind a 2 MW wind turbine. *Atmos. Environ.,* **22,** 803–820.

Ivanova, L. A., and E. D. Nadyozhina, 2000: Numerical simulation of wind farm influence on wind flow. *Wind Eng.,* **24,** 257–269, doi:10.1260/0309524001495620.

Jensen, L. E., 2007: Analysis of array efficiency at Horns Rev and the effect of atmospheric stability. *Proc. 2007 EWEC Conf.,* Milan, Italy, European Wind Energy Association.

Keith, D., J. DeCarolis, D. Denkenberger, D. Lenschow, S. Malyshev, S. Pacala, and P. J. Rasch, 2004: The influence of large-scale wind power on global climate. *Proc. Natl. Acad. Sci. USA,* **101,** 16 115–16 120, doi:10.1073/pnas.0406930101.

Kirk-Davidoff, D. B., and D. W. Keith, 2008: On the climate impact of surface roughness anomalies. *J. Atmos. Sci.,* **65,** 2215–2234.

Klemp, J. B., and R. B. Wilhelmson, 1978: The simulation of three-dimensional convective storm dynamics. *J. Atmos. Sci.,* **35,** 1070–1096.

Lu, H., and F. Porté-Agel, 2011: Large-eddy simulation of a very large wind farm in a stable atmospheric boundary layer. *Phys. Fluids,* **23,** 065101, doi:10.1063/1.3589857.

Nakanishi, M., and H. Niino, 2009: Development of an improved turbulence closure model for the atmospheric boundary layer. *J. Meteor. Soc. Japan,* **87,** 895–912, doi:10.2151/jmsj.87.895.

Nielsen-Gammon, J. W., and Coauthors, 2008: Multisensor estimation of mixing heights over a coastal city. *J. Appl. Meteor. Climatol.,* **47,** 27–43.

Poulos, G. S., and Coauthors, 2002: CASES-99: A comprehensive investigation of the stable nocturnal boundary layer. *Bull. Amer. Meteor. Soc.,* **83,** 555–581.

Rajewski, D., and Coauthors, 2013: Crop Wind Energy Experiment (CWEX): Observations of surface-layer, boundary layer, and mesoscale interactions with a wind farm. *Bull. Amer. Meteor. Soc.,* **94,** 655–672.

Schepers, J. G., T. S. Obdam, and J. Prospathopoulos, 2012: Analysis of wake measurements from the ECN Wind Turbine Test Site Wieringermeer, EWTW. *Wind Energy,* **15,** 575–591, doi:10.1002/we.488.

Skamarock, W. C., and Coauthors, 2008: A description of the Advanced Research WRF version 3. NCAR Tech. Note NCAR/TN-475+STR, 125 pp.

Svensson, G., and Coauthors, 2011: Evaluation of the diurnal cycle in the atmospheric boundary layer over land as represented by a variety of single-column models: The second GABLS experiment. *Bound.-Layer Meteor.,* **140,** 177–206, doi:10.1007/s10546-011-9611-7.

Wang, C., and R. G. Prinn, 2010: Potential climatic impacts and reliability of very large-scale wind farms. *Atmos. Chem. Phys.,* **10,** 2053–2061, doi:10.5194/acp-10-2053-2010.

——, and ——, 2011: Potential climatic impacts and reliability of large-scale offshore wind farms. *Environ. Res. Lett.,* **6,** 025101, doi:10.1088/1748-9326/6/2/025101.

Whiteman, D. C., X. Bian, and S. Zhong, 1997: Low-level jet climatology from enhanced rawinsonde observations at a site in the Southern Great Plains. *J. Appl. Meteor.,* **36,** 1363–1376.

Zhou, L., Y. Tian, S. Baidya Roy, C. Thorncroft, L. F. Bosart, and Y. Hu, 2012: Impacts of wind farms on land surface temperature. *Nature Climate Change,* **2,** 539–543, doi:10.1038/nclimate1505.